

multiclimact



D10.3 - DIGITAL SOLUTION FOR CHARACTERISATION OF THERMAL AND ENERGY SOLUTIONS

Development for the application to a real demo case

SEPTEMBER 2025 | TECNALIA RESEARCH & INNOVATION



MULTICLIMACT D10.3 - DIGITAL SOLUTION FOR CHARACTERISATION OF THERMAL AND ENERGY SOLUTIONS

Project Title	MULTI-faceted CLIMate adaptation ACTions to improve resilience, preparedness and responsiveness of the built environment against multiple hazards at multiple scales
Project Acronym	MULTICLIMACT
Contract Number	101123538
Project Coordinator	Rina Consulting S.p.A.
WP Leader:	ENEA

Deliverable	D10.3 - Digital solution for characterisation of thermal and energy solutions - development for the application to a real demo case	
DoA	Explanation in DoA	
Lead beneficiary	TECNALIA	
Main Authors	Iñigo López Villamor (TECNALIA), Vicente Mediano (CYPE)	
Main contributors	Noelia Vicente (TECNALIA), Beñat Arregi (TECNALIA), Ander Romero (TECNALIA), Bárbara Torregrosa Jaime (CYPE), Aurea Plumed (BCN)	
Reviewers	Gloria Cosoli (UNIVPM), Chiara Ormando (ENEA), Marta Rivarola (RINA-C), Celina Solari (RINA-C)	
Due date	30.09.2025	
Report date	22.09.2025	
Version	3	

Document classification	PU Public
-------------------------	-----------



REVISION TABLE

Version	Date	What	
V0.1	27.11.2024	Table of contents and structure	
V0.2	01.04.2025	First sections populated	
V1	21.07.2025	First draft ready for internal revision	
V2	25.08.2025	Final version ready for coordinator quality check	
V3	22.09.2025	Final version ready for submission	

Copyright Notices
©2023-2027 MULTICLIMACT Consortium Partners. All rights reserved.
MULTICLIMACT is a Horizon Europe project supported by the European Commission under grant agreement No 101123538.
Views and opinions expressed are however those of the author(s) only and do not necessarily reflect those of the European Union. Neither the European Union nor the granting authority can be held responsible for them.
All information in this deliverable may not be copied or duplicated in whole or part by any means without express prior agreement in writing by the MULTICLIMACT

partners.

All trademarks and other rights on third party products mentioned in this document are acknowledged and owned by the respective holders.

The MULTICLIMACT consortium does not guarantee that any information contained herein is error-free, or up to date, nor makes warranties, express, implied, or statutory, by publishing this document.





TABLE OF CONTENTS

REVISION TABLE	3
Executive Summary	9
1. Introduction	10
1.1. Purpose and target group	10
1.2. Contributions of partners	10
2. Overall approach	11
2.1. Structure of the deliverable	11
2.2. Interaction with other tasks	11
3. Objectives and expected impact	12
3.1. Objectives	12
3.1.1. Physics based digital tool	12
3.1.2. Data-driven digital tool	12
3.2. Expected impact	13
3.2.1. Physics-based digital tool	13
3.2.2. Data-driven digital tool	13
4. Background and context	15
4.1. Previous works	15
4.1.1. Physics-based digital tool	15
4.1.2. Data-driven digital tool	17
4.2. Application within the project	17
4.2.1. Demonstration pilot	17
5. Workflow and development	19
5.1. Physics-based modelling tool	19
5.1.1. Workflow design	19
5.1.2. Pavement simulation tests	20
5.1.3. Urban simulation tests	23
5.2. Data-driven digital tool	26
5.2.1. Manual calibration of RC models	26
5.2.2. KPI of the data-driven digital too	27
6. Results	29
6.1. Physics-based modelling tool	29
6.1.1. Surface temperature	29
6.1.2. Heat transfer rate through paven	nent32
	34
6.1.4. Cooling and heating demand of a	djacent buildings37
6.1.5. Indoor operative temperature	38

D10.3 - Digital solution for characterisation of thermal and energy solutions

Deviations to the Plan48

great solution for characterisation of thermat and energy solutions	
Data-driven digital tool	40
Testing dataset	41
Results of data-driven digital tool	43
Comparison vs manually calibrated RC model	46

Cod	unde	رط ام		

the European Union

6.2.

7. 8.

9.

6.2.1.

6.2.2.

6.2.3.



LIST OF TABLES

Table 1. Contributions of partners	10
Table 2. Absorptance variation cases used in the simulation tests	23
Table 3. Conductivity variation cases used in the simulation tests	23
Table 4. EPW ambient temperature variations cases used for urban simulations	
Table 5. Direct models according to ISO 13790	
Table 6. Detailed clear sky models, where εsky [-] is the sky emissivity, Tdp [°C] the dev	
point temperature, TA [°C] ambient temperature, and Pv [mb] the vapor pressure	
Table 7. Peak surface temperature results for absorptance iterations	
Table 8. Peak surface temperature results for conductivity iterations	
Table 9. Peak heat transfer rate through pavement results by absorptance iterations	
Table 10. Peak heat transfer rate through pavement results for conductivity and hybrid	
iterations	
Table 11. Peak heat emission to air results for absorptance iterations	
Table 12. Peak heat emission to air results by conductivity and hybrid iterations	
Table 13. EPW ambient temperature variations cases used for urban simulations	
Table 14. Peak indoor maximum comfort temperature results for EPW file variations	
Table 15. Peak indoor minimum comfort temperature results for EPW file variations	
Table 16. Statistical comparison of measured temperature values	
Table 17. Evaluation metrics of all identified RC models	
Table 18. Evaluation metrics of all manually identified RC models	46
LIST OF FIGURES	
Figure 1. Interaction of task 10.3 with other tasks of the project (CREDITS: TECNALIA)	11
Figure 2. Previous Workflow depending on external tools for BIM and Analytical models (CREDITS: CYPE)	15
Figure 3. Improved Workflow with the integration of 3D modelling within CYPETHERM (CREDITS: CYPE)	
Figure 4. New CYPETHERM Interface with the integration of urban contexts (CREDITS: CYPE)	
Figure 5. Google Maps and Street View images of Carles Pirozzini Street (left) and Passeig Santa Eulalia (righ Figure 6. General workflow for the physics-based modelling tool (CREDITS: CYPE)	
Figure 7. Barcelona's current pavement solution, according to D4.3. (CREDITS: CYPE)	
Figure 8. Pavement section modelled in the '3D model' tab, within CYPETHERM interface (CREDITS: CYPE)	
Figure 9. Physical and thermal properties of the pavement layers solution, within CYPETHERM interface (CRED	NTS:
CYPE)	
Figure 10. Pavement section ready for simulation in the 'Energy simulation' tab (CREDITS: CYPE) Figure 11. Urban environment created using CYPETHERM's 3D model tab (CREDITS: CYPE)	
Figure 12. Building envelope layers defined for the simulation (CREDITS: CYPE)	
Figure 13. Internal operational settings for the building simulations (CREDITS: CYPE)	
Figure 14. Graphical representation of the EPW file data within CYPETHERM Eplus (CREDITS: CYPE)	
Figure 15. EPW file modification for 1 °C decrease (CREDITS: CYPE)	
Figure 16. Hourly surface temperature variation by absorptance iteration (CREDITS: CYPE)	
Figure 17. Hourly surface temperature variation by conductivity and hybrid iterations (CREDITS: CYPE) Figure 18. Hourly heat transfer rate through pavement by absorptance iterations (CREDITS: CYPE)	
rigure 18. Hourly heat transfer rate through pavement by absorptance iterations (CREDITS: CYPE) Figure 19. Hourly heat transfer rate through pavement by conductivity and hybrid iterations (CREDITS: CYPE) .	
Figure 20: Hourly heat emission to air by absorptance iterations (CPEDITS: CVPF)	37

D10.3 - Digital solution for characterisation of thermal and energy solutions



Figure 21. Hourly heat emission to air by conductivity and hybrid iterations (CREDITS: CYPE)	36
Figure 22. Monthly indoor maximum comfort temperature (CREDITS: CYPE)	39
Figure 23. Monthly indoor minimum comfort temperature (CREDITS: CYPE)	40
Figure 24. Layout of the three pavement samples monitored in Barcelona (CREDITS: COMSA)	41
Figure 25. Temperature sensor distribution (CREDITS: COMSA)	42
Figure 26. Time-series plot of all 4 monitored surface temperatures, their average value, and ambient	
temperature (top), and solar irradiation (bottom) (CREDITS: TECNALIA)	42
Figure 27. Subset of possible topologies of the optimal model: 1 node RC model (left), 2 nodes RC model	
(middle), 3 nodes RC model (right) (CREDITS: TECNALIA)	43
Figure 28. Algorithm for automated pavement model selection (CREDITS: TECNALIA)	44
Figure 29. Time-series plots of observed versus predicted temperature values, residuals, ambient temperature	
(Ta), and solar irradiation (Ps) for a typical summer week (CREDITS: TECNALIA)	45
Figure 30. Time-series plots of observed versus predicted temperature values, residuals, ambient temperature	
(Ta), and solar irradiation (Ps) for a cloudy period (CREDITS: TECNALIA)	46
Figure 31. Time-series plots of observed versus predicted (manually calibrated) temperature values, residuals,	
ambient temperature (Ta), and solar irradiation (Ps) for a typical summer week (CREDITS: TECNALIA)	47
Figure 32. Time-series plots of observed versus predicted (manually calibrated) temperature values, residuals,	,
ambient temperature (Ta), and solar irradiation (Ps) for a cloudy period (CREDITS: TECNALIA)	47



Abbreviations and Acronyms

ACRONYM	DESCRIPTION	
AIC	Akaike Information Criterion	
BIC	Bayesian Information Criterion	
ВІМ	Building Information Modelling	
CTSMR	Continuous Time Stochastic Modelling for R	
DTU	Danish Technical University	
EPW	EnergyPlus Weather	
HVAC	Heating, Ventilation, and Air Conditioning	
IFC	Industry Foundation Classes	
KPI	Key Performance Indicators	
MAE	Mean Absolute Error	
QLWD	Measured longwave radiation	
R ²	Coefficient of Determination	
RC	Resistance-Capacitance	
RMSE	Root Mean Square Error	
σ	Stefan-Boltzmann constant	
T _A	Ambient Temperature	
T _{OP}	Operative Temperature	
TR	Radiant Temperature	
T _{sky}	Sky Temperature	
UHI	Urban Heat Island	



Executive Summary

The MULTICLIMACT project aims to develop a mainstreamed framework and a tool for supporting public stakeholders and citizens to assess the resilience of the built environment and its people at multiple scales (buildings, urban areas, territories) against locally relevant natural and climatic hazards and supply-chains, as well as to support them to enhance their preparedness and responsiveness across their life cycle. The mainstreamed approach will include a method specifically targeted for including several types of built environment assets, including human wellbeing, health, and quality of life as an essential scale of analysis and action. MULTICLIMACT will support resilience enabling actions by implementing a toolkit of 18 reliable, easy-to-implement and cost-effective Design methods, Materials, and Digital Solutions, enabling users to easily estimate the impact of their implementation on the resilience of the targeted asset, integrating a multidisciplinary approach integrating socio-economic, life, engineering, and climate disciplines.

Deliverable D10.3 specifically addresses the final design of a pair of digital solutions for climate-proof characterization of thermal and energy solutions, more specifically a physics-based digital tool and a data-driven digital tool.

The physics-based digital tool, based on the existing tool CYPETHERM Eplus ('CYPETHERM Eplus') developed by CYPE, aims to expand its scope capturing the interaction between multiple buildings and their surrounding pavements. This tool will use Building Information Modelling (BIM) to replicate the urban context including the technical data of its materials. The data-driven digital tool, on the other hand, is based on a semi-empirical model generator that, using monitored data, will generate models to assess the actual in situ performance of pavement solutions.

Both digital tools have been tested in relevant scenarios. Given the actual unavailability of the definitive location of the Spanish demo, the validation of the physics-based digital tool has been carried out by modelling one hypothetical location of the demo in the city of Barcelona. On the other hand, as for the data-based digital tool, its validation has been carried out using monitored data from one of the samples developed and monitored at COMSA's facilities.

Tecnalia is involved in this work as the leader of the task and as the developer of the data-driven tool. CYPE is responsible for the development of the physics-based modelling tool. BCN is involved as the responsible for the demo site.



1. INTRODUCTION

This document, D10.3 "Digital solution for characterisation of thermal and energy solutions - Development for the application to a real demo case", is a deliverable of the MULTICLIMACT project, funded by the European Union Horizon Europe Program (2021 - 2027) under Grant Agreement No. 101123538.

1.1. PURPOSE AND TARGET GROUP

The present report summarises the work performed in task 10.3, where the final design of two different digital tools has been developed, as well as their adaptation to the application to the Spanish demo site. The first of the tools relies on physics-based models to predict the performance of different interventions in terms of their thermal performance, primarily aimed at the design stage. The second of the tools is based on a data-driven model generator that seeks to characterise the actual performance of interventions from monitored data. Together, they provide different but complementary perspectives to support informed design decisions and enhance urban resilience under extreme heat.

The final designs of the digital tools included in this document correspond to WP10 task 10.3, which belongs to the second phase of the project, from M13 to M30. The two digital tools mentioned in this document are expected to be further tested in future work packages, concretely in tasks 11.2 and 15.2.

1.2. CONTRIBUTIONS OF PARTNERS

The following Table 1. *Contributions of partners* depicts the main contributions from project partners in the development of this deliverable.

PARTNER SHORT NAME	CONTRIBUTIONS
TECNALIA	Overall structure of the document, main contributor of sections 1, 2, 3.1.2, 3.2.2, 4.1.2, 5.2, 6.2, 7, 8 and 9.
СҮРЕ	Main contributor of sections 3.1.1, 3.2.1, 4.1.1, 4.2, 5.1, 6.1 and 9.
BCN	Main contributor of section 4.2 and 9.

Table 1. Contributions of partners



2. OVERALL APPROACH

2.1. STRUCTURE OF THE DELIVERABLE

The present deliverable consists of eight sections, containing an introduction, the overall approach of the task, and the four main sections of the document: the objectives and expected impact of both digital tools, a summary of the work done during the first phase of the project, and finally, the workflow and development, and results for the physics-based and data-driven digital tool. The document concludes with two sections, one dedicated to the deviations to the plan and another on the task's conclusions.

The objectives and expected impact section describes the objectives of the whole task, as well as the specific objectives and expected impact for each of the digital tools.

The remaining sections of the document cover the work completed during the previous project phase to establish the initial state of both tools, the workflow carried out in the second year, the results achieved from the final design of both tools, the deviations from the planned work, and the conclusions drawn from the task.

2.2. INTERACTION WITH OTHER TASKS

The deliverable D10.3 refers to the work done in task 10.3 "Digital solution for characterisation of thermal and energy solutions - development for the application to a real demo case". This task continues the works done during the first phase of the project, in task 4.3, where the initial design of two digital solutions was developed. As it is shown in Figure 1, their design and adaptation to be tested in the Spanish demo site is expected to be done in task 10.3 and tested and validated in tasks 11.2 and 15.2. In addition to the tasks shown in the figure, which are the ones that have a direct relationship with the digital tools developed in T10.3, data obtained from T9.2 has been used to test and validate the development of the data-driven digital tool.

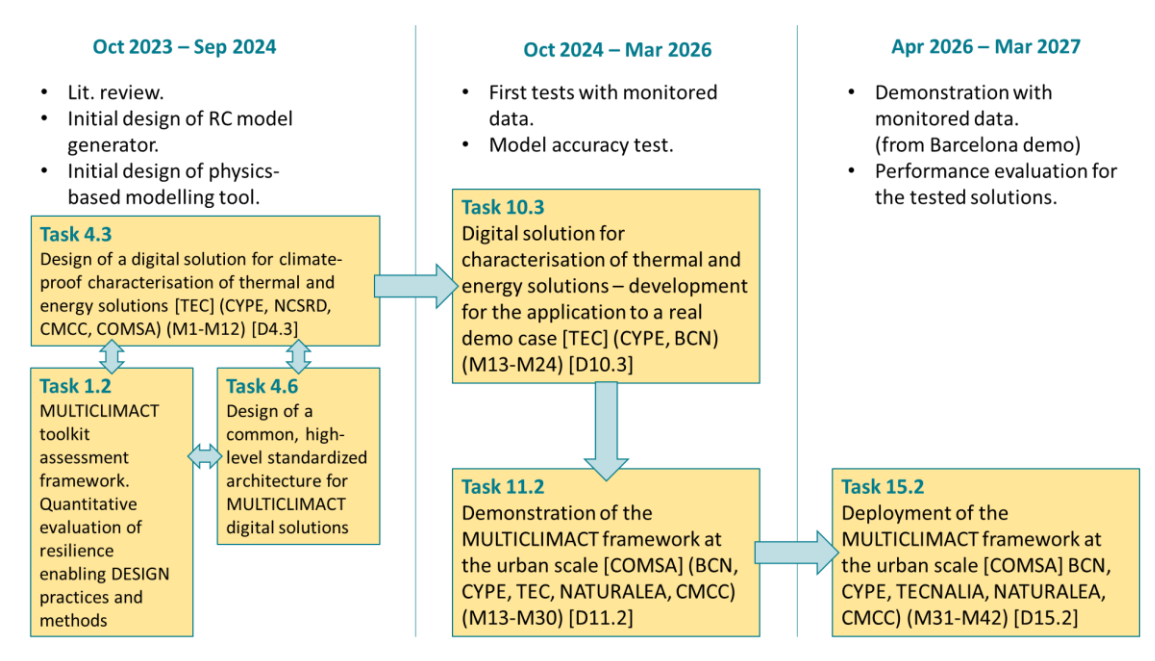


Figure 1. Interaction of task 10.3 with other tasks of the project (CREDITS: TECNALIA)



3. OBJECTIVES AND EXPECTED IMPACT

3.1. OBJECTIVES

This task focuses on the development of two digital tools designed to assess the thermal performance of urban pavements and their impact on the energy behaviour of surrounding buildings. The underlying objective is to support climate adaptation strategies through reliable and replicable modelling approaches.

Each of the tools is based on a different approach and aimed at a different stage of the intervention. While the first tool uses physics-based models to evaluate the effectiveness of interventions at the design stage, the second tool is based on data-driven models to characterise the actual in-situ performance of the modelled interventions using monitored data. Therefore, both tools will provide complementary perspectives to support informed design decisions and improve the resilience of urban environments under extreme heat conditions.

3.1.1. PHYSICS BASED DIGITAL TOOL

The main objective of this task regarding the physics-based modelling tool is to conclude and test its development, based on the design presented in Deliverable 4.3 "Design of a digital solution for climate proof characterisation of thermal and energy solutions". The resulting implementation was integrated within the CYPETHERM EPlus ('CYPETHERM EPlus') software environment. Additionally, beyond simply improving the software functionality, this task aims to ensure a logical and practical modelling workflow. This workflow will be able to deal with geometrical configurations of urban contexts. These improvements are essential for optimise and simplify thermal simulations of pavements and their impact on building energy consumptions in urban environments.

As described in D4.3, the main improvement of CYPETHERM Eplus involved incorporating 3D modelling capabilities directly into the software. This represents a significant shift from the traditional workflow, which required the use of external software to generate analytical models. Previously, CHYPETHEM Eplus depended on analytical models produced in tools such as IFC Builder and Open BIM Analytical Model or imported from external BIM tools. The new approach enables directly handling of 3D geometry within CYPETHERM, eliminating the need for external processing steps and optimising the entire model pipeline.

Regarding the simulation strategy, the objective is to test and prove the correct functioning of the two-stage workflow described in the previous task. First, pavement surface temperatures were simulated based on material properties and climate data. Then, the effect on energy demand in surrounding building was simulated using this output. The test simulations were carried out to verify the accuracy and completeness of the whole workflow, and to ensure that the system was functioning as intended prior of its use in the Spanish demo case.

3.1.2. DATA-DRIVEN DIGITAL TOOL

The accurate forecasting of pavement surface temperature, or of Key Performance Indicators (KPIs) related to it, is essential for both the design and performance assessment of pavement solutions. Traditionally, data-driven models applied in pavement contexts are black-box in nature, leveraging historical data such as air temperature, solar radiation, wind speed and direction, and pavement surface temperature (Tabrizi et al.). However, this approach is still not widely adopted for predicting pavement surface temperature, an area where physical models remain the predominant choice.

The developed data-driven digital tool is designed to streamline the modelling process required to characterize the thermal behaviour of soils and pavement solutions. Central to the tool is an automated resistance-capacitance (RC) model generator, which significantly reduces the need for



specialized expertise and the time typically required for model calibration. Moreover, the tool also computes comfort-related KPIs, such as operative temperature, enabling early evaluation of a given pavement solution's thermal response to extreme heat events.

3.2. EXPECTED IMPACT

The development of these digital tools is expected to significantly improve the efficiency and accessibility of the implementation of climate adaptation strategies in urban settings, specifically in relation to heat island effect mitigation and building energy demand. The tools will provide practical indicators on the thermal behaviour of pavements and the resulting energy performance of surrounding buildings.

This democratisation of modelling capabilities will enable wider adoption among practitioners, including public authorities and infrastructure designers. In addition, the integrated calculation of comfort-related KPIs enables more informed decisions regarding climate resilience and user comfort, ultimately contributing to the development of more sustainable and climate-adapted urban infrastructures.

3.2.1. PHYSICS-BASED DIGITAL TOOL

The physics-based digital tool developed within CYPETHERM EPlus software is expected to make a significant contribution to the evaluation and optimisation of climate-adaptative design and solutions. By simulating thermal interactions at urban scale, the tool enables the quantification of the impact of pavement materials, street layout, and urban context on local microclimate and building design.

Its most direct impact lies in its ability to generate scenario-based results that quantify the effects of interventions such as reflective coatings, permeable pavements, or alternative materials. This will enable urban planners, engineers, and designers to evaluate performance indicators, such as surface temperature variations, heat transfer rates, differences in building energy use, and operative thermal comfort.

A key innovation is the integration of BIM-based modelling of buildings and construction elements within CYPETHERM Eplus, eliminating the need for external analytical models generation. This results in a more efficient and user-friendly workflow that reduces modelling time and complexity. This workflow enables professionals to produce simulations with less risks of errors, thus improving accessibility and usability.

Additionally, adopting open data models, such as IFC an JSON, ensures interoperability with commonly used BIM processes and other modelling or visualisation tools. This design choice allows for the potential of the tool to be replicated and adapted in projects beyond the Spanish demo case that is the core application of the proposed solutions. Also, the software architecture supports the incorporation of different modelling workflows, combining physical simulations with data-driven input, offering flexibility for future validation or calibration efforts.

Finally, in a broader scope, this tool provides a robust solution for evidence-based, predictive urban design, supporting public authorities and stakeholders in optimising their strategies in terms of thermal comfort, energy efficiency, and resilience to climate change.

3.2.2. DATA-DRIVEN DIGITAL TOOL

The developed data-driven digital tool will facilitate the wider adoption of data-driven approaches in pavement thermal analysis, effectively bridging the gap between theoretical white-box models and real-world performance. By providing easy-to-use and intuitive tools, the tool will lower the barrier to entry for practitioners, enabling a more accurate assessment of actual pavement performance, rather than relying solely on theoretical predictions. The automation of model generation will also

D10.3 - Digital solution for characterisation of thermal and energy solutions



reduce the need for specialized expertise, making it more accessible to a broader range of users.

This, in turn, will enable a more informed evaluation of pavement design and implementation as well as a more effective assessment of climate adaptation strategies. The practical application of data-driven models will also facilitate the identification of potential discrepancies between theoretical assumptions and real-world behaviour, allowing for the refinement and validation of theoretical models. Furthermore, by leveraging the strengths of both data-driven and physical approaches, the tool will contribute to the development of more accurate and reliable models, ultimately leading to the design and implementation of more sustainable, climate-resilient, and user-friendly urban infrastructures. Additionally, the generation of easily interpretable comfort-related KPIs, such as operative temperature, will make the tool accessible to professionals with varying levels of expertise, thereby promoting a more data-driven and inclusive approach to pavement design and management.



4. BACKGROUND AND CONTEXT

4.1. PREVIOUS WORKS

4.1.1. PHYSICS-BASED DIGITAL TOOL

By the end of Task 4.3, the conceptual and architectural framework of the physics-based modelling tool had been partially implemented and prototyped. The tool logic, structure, and purpose within the MULTICLIMACT project had been validated theoretically, and a pre-alpha version had been developed to test the new functionalities internally.

At that stage, the adaptation of CYPETHERM Eplus to the project requirements was underway but not yet fully completed. Specifically, the integration of 3D modelling capabilities directly within the software was still under development, with no stable version available yet. As stated in D4.3, by then the software was not able to generate analytical models from Industry Foundation Classes (IFC) models and depended on external tools to carry out this need. This reliance on external software limited the usability and flexibility of the modelling process.

Additionally, the possible workflows for energy simulations could vary depending on the BIM Authoring tool used (Figure 2). Within CYPE ecosystem, IFC Builder allowed a direct connection to CYPETHERM EPlus, without the need to generate an analytical model. However, when dealing with more complex geometry, CYPE Architecture was a more optimal option. In this case, an analytical model had to be created via the Open BIM Analytical Model tool before being used in CYPETHERM EPlus. On the other hand, when external BIM authoring tools were used, the process required exporting the IFC file and uploading it through the IFC Uploader tool. In these cases, as with CYPE Architecture, generating an analytical model became mandatory before conducting the energy simulation. Regardless of the tool, the final output was an energy simulation report generated by CYPETHERM EPlus.

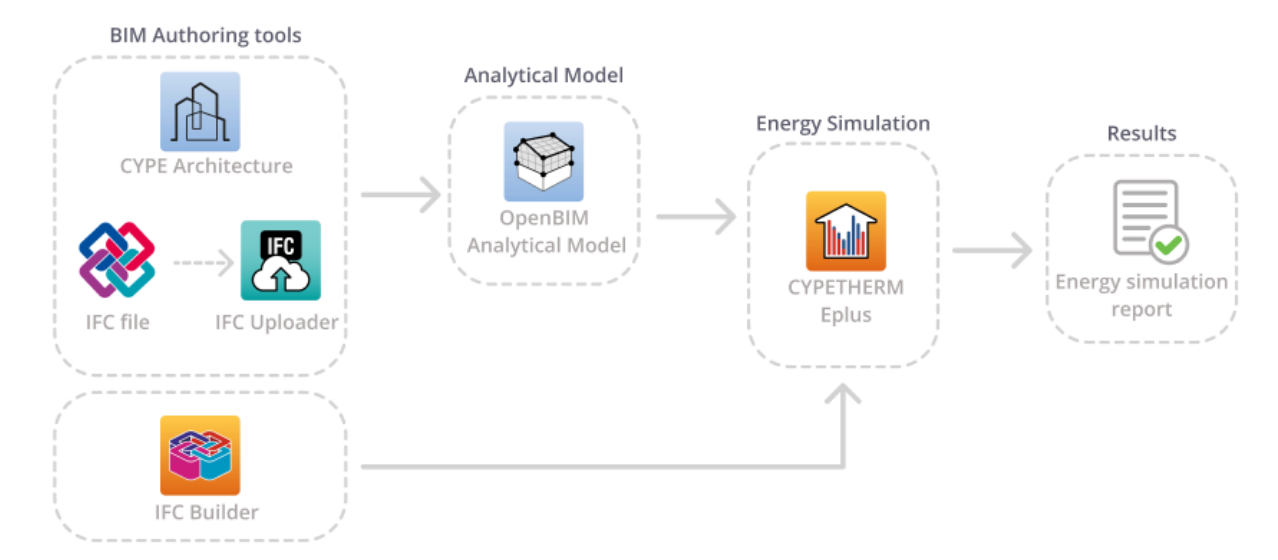


Figure 2. Previous Workflow depending on external tools for BIM and Analytical models (CREDITS: CYPE)

With the incorporation of IFC Builder functionalities directly into CYPETHERM EPlus, as well as the native generation of analytical models within the same environment, the workflow for energy simulations was significantly simplified (Figure 3). Users no longer need to rely on external tools to prepare the geometry or generate analytical models, as both tasks can now be carried out within CYPETHERM itself. This streamlined the overall process, reduced potential compatibility issues, and



enabled a more integrated user experience. This simplified workflow was achieved by incorporating planned improvements into the software.

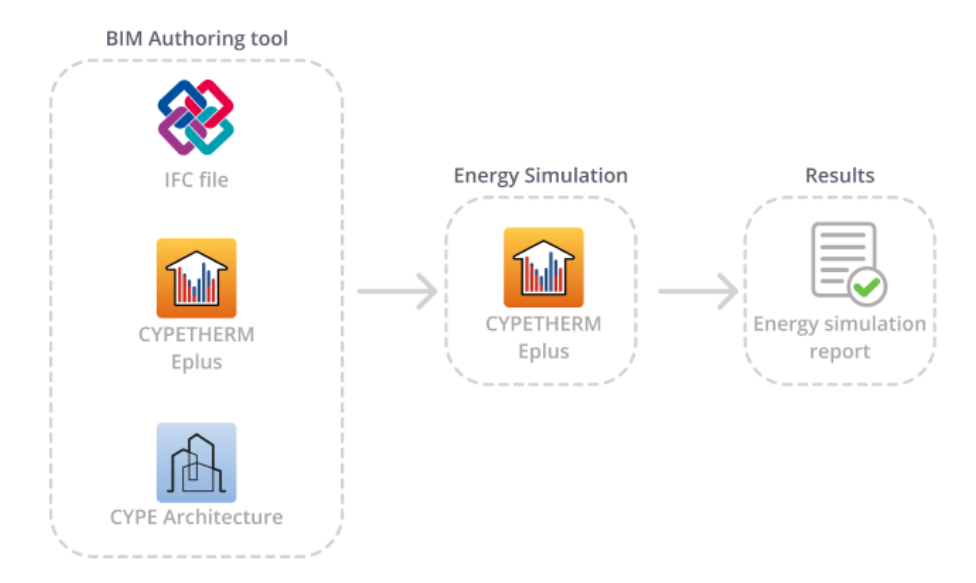


Figure 3. Improved Workflow with the integration of 3D modelling within CYPETHERM (CREDITS: CYPE)

These planned improvements included upgrading the CYPETHERM interface (Figure 4) to include new modules, such as the '3D Model' and 'Thermal Model' tabs, for the geometrical definition of projects and energy analyses respectively. This allows users to define geometry and simulation parameters without switching environments. These improvements were essential in transforming CYPETHERM from a tool for specific buildings that depended on external tools to a versatile simulation capable of even addressing urban-scale interventions.

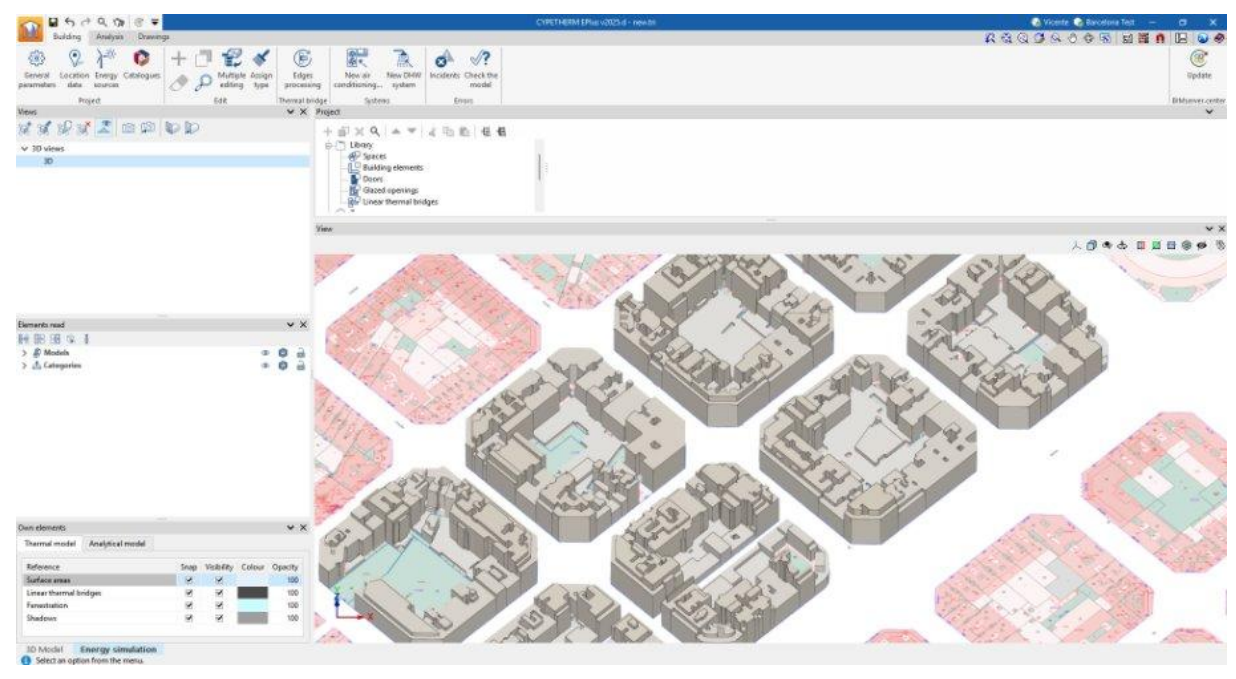


Figure 4. New CYPETHERM Interface with the integration of urban contexts (CREDITS: CYPE)



4.1.2. DATA-DRIVEN DIGITAL TOOL

The first design and preliminary tests of the RC model generator that is the core of the digital tool have been carried out during the first year of the project, in task 4.3.

In the preliminary design phase of the digital tool, information criteria (Schwarz) have been chosen to select the most suitable model until a final evaluation of the solution can be conducted. Two of the most widely used information criteria for determining the optimal model order are the Akaike Information Criterion (AIC) and the Bayesian Information Criterion (BIC) (Lopez-Villamor et al.). These criteria are comparative metrics, meaning they are used to compare models rather than evaluate a single model on its own. The formulation of both AIC and BIC is given in Eq. (1) and Eq. (2).

$$AIC = -2L + 2 \cdot k \tag{1}$$

$$BIC = -2L + k \cdot Ln(n) \tag{2}$$

where L is the log likelihood function of the model evaluated at the maximum likelihood estimate, k is the number of estimated parameters, and n is the number of datapoints.

In addition, in task 4.3 the KPI chosen as the main output of the digital tool was the Operative Temperature. This parameter, calculated by the digital tool using as an input the predicted surface temperature values, as well as other meteorological parameters, reflects the combined influence of air temperature and radiant heat exchange on human comfort.

4.2. APPLICATION WITHIN THE PROJECT

4.2.1. DEMONSTRATION PILOT

By the time of writing this deliverable, the exact location for the demonstration pilot in Barcelona has not yet been confirmed. However, the selection process is underway, and several candidate sites have been assessed based on criteria such as exposure, urban geometry, limited traffic intensity, and proximity of surrounding buildings.

From the original set of 8 possible sites identified in D4.3, two final locations are currently under consideration (Figure 5), each with distinct characteristics in terms of shading, orientation, and building layout. These two final locations are the one located in Carles Pirozzini Street (between Collserola and Enginyeria streets) and Passeig Santa Eulàlia (between General Vives and Cancarelleu streets) both in the western zone. Discussions among the project partners are ongoing to determine which site offers the most suitable conditions for testing the proposed pavement interventions and collecting consistent, comparable data.











Figure 5. Google Maps and Street View images of Carles Pirozzini Street (left) and Passeig Santa Eulalia (right).

Despite the lack of a final decision, initial evaluations suggest that one of the candidate locations offers a more favourable solar profile and thermal exposure throughout the day, making it potentially more suitable for assessing the impact on new pavement materials on microclimate and adjacent buildings. This location corresponds to the one in **Carles Pirozzini Street**. The assessment will be finalised in the coming weeks, in coordination with local stakeholders, namely Barcelona Municipality and COMSA.

For Task 10.3, and to complete the development and internal testing of the physics-based modelling workflow, an **arbitrary urban scenario in Barcelona** has been simulated to represent a realistic test scenario. This allows the modelling process to be fully implemented and verified ahead of the final demo deployment. Once the official pilot location is confirmed, the same workflow will be applied using the actual geometry and site-specific input data during Tasks 11.2 and 15.2.



WORKFLOW AND DEVELOPMENT

5.1. PHYSICS-BASED MODELLING TOOL

In line with the structure described in D4.3, the work carried out in Task 10.3 regarding the physics-based modelling tool was centred on integrating and refining the features of CYPETHERM EPlus to facilitate a full urban-scale simulation workflow. As mentioned earlier, the core improvement of the task was the ability to perform geometric modelling and energy simulation on the same environment, eliminating the need for external analytical model generation.

To prove these advancements were functioning correctly, a workflow was designed and tested for carrying out the simulations. The functioning workflow will be used in the future for the Barcelona demo case in subsequent tasks (T11.2 and T15.2), assuring replicability in real-world scenarios. As a significant aspect, it considered the modelling of all the simulation geometry within CYPETHERM.

5.1.1. WORKFLOW DESIGN

The designed workflow (Figure 6) consisted in **four steps** within two different types of simulations. Each of these steps represented a necessary stage for evaluating and comparing the thermal performance of existing and proposed pavement solutions, and their resulting impact on the energy behaviour of surrounding buildings. The first part of the process focused on assessing how different **pavement materials** respond to climatic conditions, while the second part considers also the surrounding **urban environment** to estimate the influence of pavement thermal performance on nearby buildings.

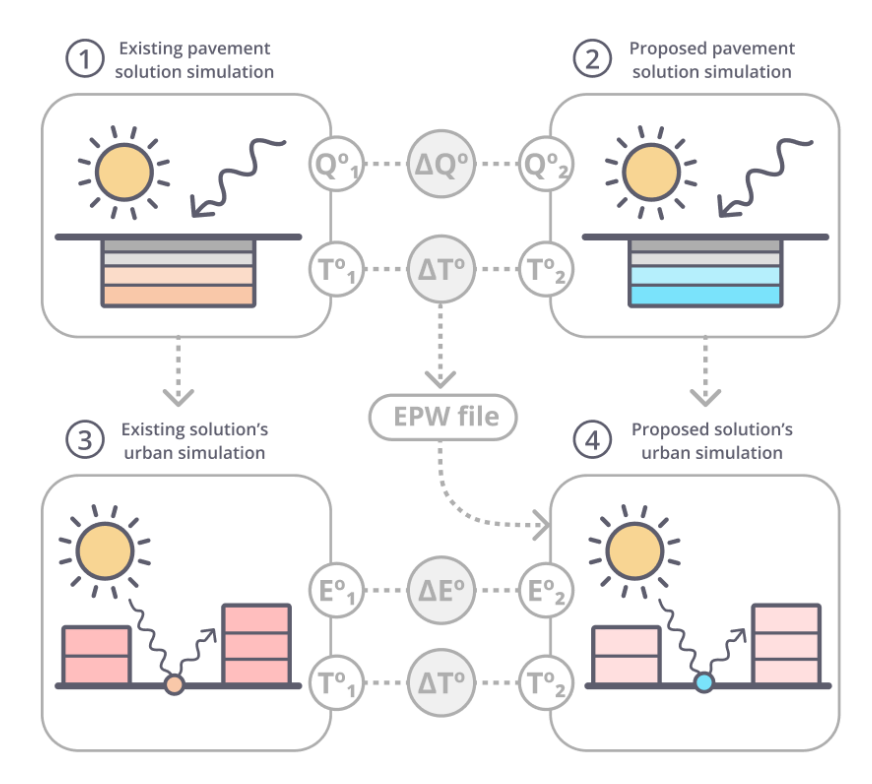


Figure 6. General workflow for the physics-based modelling tool (CREDITS: CYPE)

For the first stage, the definition of the existing geometry, physical properties of the existing pavement solution (including thickness, material layers, and thermal properties such as conductivity,



absorptivity, density, and specific heat), and the import of climate data to run the simulations were done. For this first simulation, Barcelona's typical asphalt solution described in D4.3 was modelled. The most relevant output for this stage is a **temperature value**, that represents the current situation of Barcelona's pavement thermal behaviour (step 1).

Then, the proposed pavement solution was modelled, and the same type of simulation was done. Here, a second **temperature value** was obtained, this time representing the projected behaviour of the pavement (step 2). The comparison of results from steps 1 and 2, namely the **temperature difference** reached by the pavement surface and layers, provided a first estimation of the effectiveness of the new design in mitigating heat accumulation.

The simulations output from steps 1 and 2 served as the basis for the urban context simulations in steps 3 and 4. Specifically, the variation in pavement temperatures was used to modify the EnergyPlus Weather (EPW) file by adjusting temperature inputs or incorporating modified environmental conditions. This allowed the representation of how local microclimate shifts caused by pavement interventions could affect building performance in the same setting.

Following this, the next stage consisted of urban-oriented simulations. A simplified urban model was created by **modelling building geometry** within CYPETHERM EPlus. For each case, existing (step 3) and proposed (step 4), the same geometry was used, but the conditions were updated according to the thermal differences observed in the previous steps. The simulation focused on evaluating the buildings response to the different pavement-induced environmental conditions.

In both simulation blocks, key performance indicators were generated and compared. From steps 1 and 2, the primary output was surface temperature evolution and heat flux through the pavement layers. From steps 3 and 4, the outputs focused on **indoor operative temperatures**, **heating and cooling energy demand**, and **overall heat exchange** between building and environment. The comparison between existing and proposed scenarios in both stages helped to quantify the thermal and energy benefits of the new pavement solution.

As this task is demonstrative in nature, and the precise material values of the proposed solution are not yet available or required at this stage, simulations (2) and (4) were performed through **multiple iterations** by varying input parameters at consistent rates. This approach allows for isolated analysis of results and provides a clearer understanding of how different material properties influence the thermal behaviour of urban environments.

5.1.2. PAVEMENT SIMULATION TESTS

To evaluate the performance of the newly integrated simulation capabilities in CYPETHERM EPlus, a series of tests were carried out using **Barcelona's current pavement solution** as the base model. This solution, defined in deliverable D4.3, includes a layered structure composed of surface and base asphalt courses, a concrete base, a granular sub-base, and compacted soil (Figure 7). This configuration was used as the reference case for all the subsequent simulations.



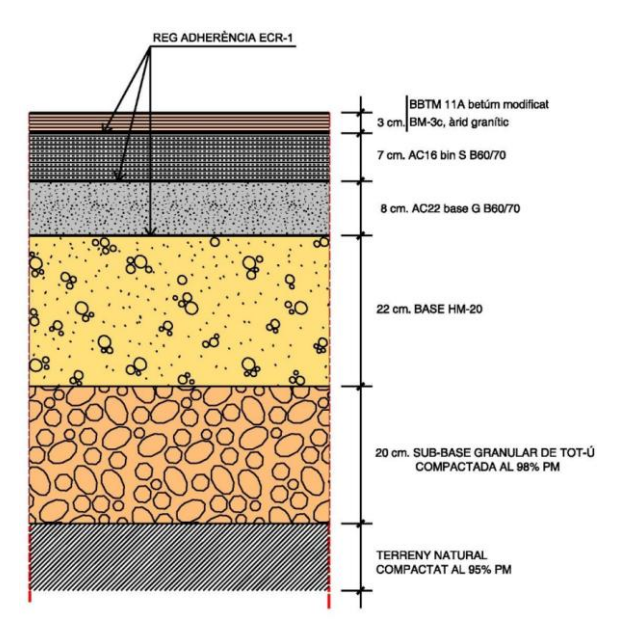


Figure 7. Barcelona's current pavement solution, according to D4.3. (CREDITS: CYPE)

Using CYPETHERM's new 3D modelling interface, the geometry of the pavement section was recreated directly within the software environment (Figure 8). The geometry was created in the '3D Model' tab, allowing for the **precise definition of the layered pavement composition** without relying on external modelling tools. This direct modelling capability is essential for developing full simulation workflows entirely within CYPETHERM and represents a key advancement introduced during Task 4.3.

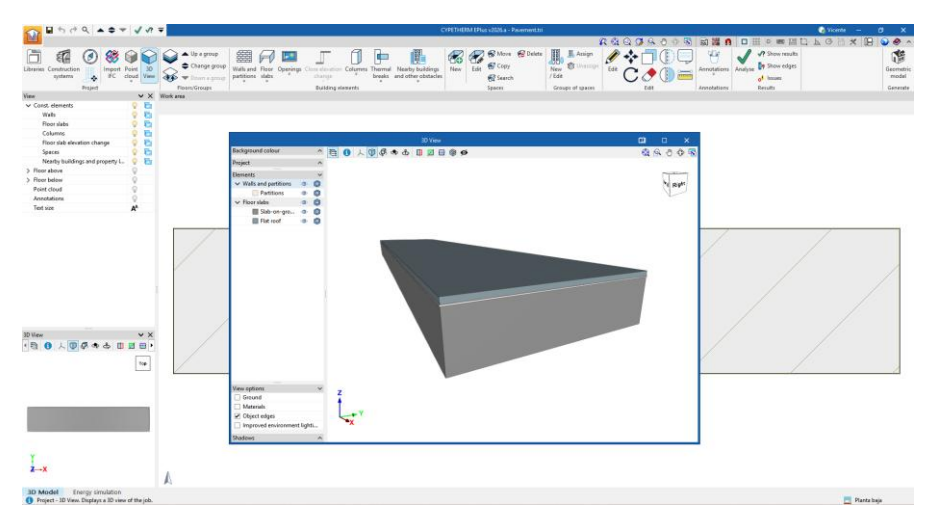


Figure 8. Pavement section modelled in the '3D model' tab, within CYPETHERM interface (CREDITS: CYPE)

Once the geometry was defined, each material layer was assigned its corresponding **physical and thermal properties** in the 'Energy simulation' tab (Figure 9). Parameters such as thickness, conductivity, thermal resistance, density, and specific heat were entered according to the reference values described in D4.3. The **absorptance of the surface** layer was also defined here, with a default value of 0.9 for the base case. This configuration allowed the model to reproduce the real-world thermal behaviour of the pavement system as accurately as possible.



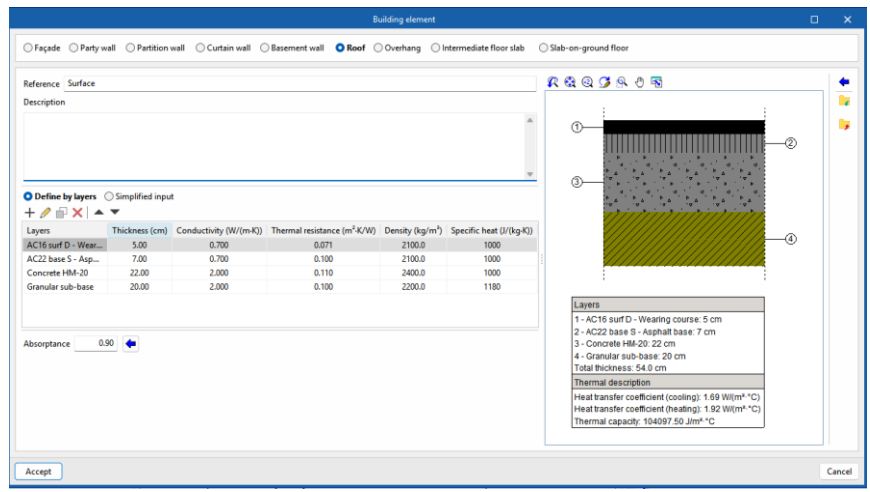


Figure 9. Physical and thermal properties of the pavement layers solution, within CYPETHERM interface (CREDITS: CYPE)

With the pavement fully defined and all input parameters configured, the model was prepared for simulation (Figure 10). For this type of test (steps 1 and 2 of the general workflow) the 'Energy simulation' tab enabled the surface-level thermal analysis based on standard climate files for Barcelona. This step represents the preliminary output values for surface temperature evolution and heat transfer through the pavement system.

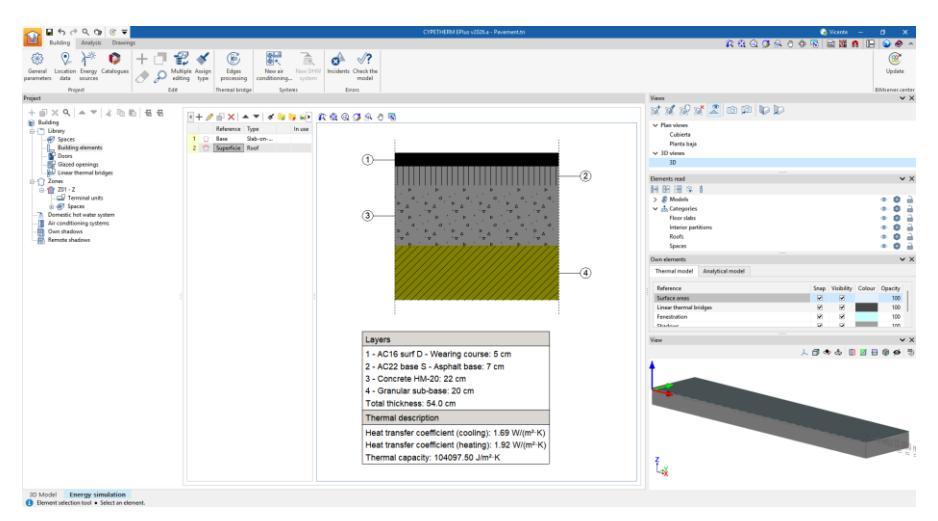


Figure 10. Pavement section ready for simulation in the 'Energy simulation' tab (CREDITS: CYPE)

To test the sensitivity of the tool and explore how different material configurations affect the thermal behaviour of urban pavements, a series of simulation iterations were conducted. This approach also served to validate the consistency and reliability of the tool across varied inputs, and to reproduce a preliminary range of expectations ahead of real-world testing. Within the presented workflow in section 5.1.1, the base simulation would represent step 1, while each iteration would be a variation of step 2.

The two key parameters evaluated in these iterations were **absorptance** and **thermal conductivity**. For the absorptance tests (Table 2. *Absorptance variation cases used in the simulation tests*), four proposed scenarios were defined by decreasing the surface absorptance value from 0.9 (base case, in step 1) down to 0.6, in 0.1 intervals (step 2 iterations). These cases correspond to conceptually increasing **albedo values** (which is the proportion of light or radiation reflected by a surface,



therefore the **inverse concept of absorptance**), allowing the effect of more reflective surfaces to be analysed.

Absorptance variation cases			
Iteration (Step) Absorptance Conductivity (W/m-			
Base (1)	0.9	0.7	
0.1 decrease (2) _a	0.8	0.7	
0.2 decrease (2) _b	0.7	0.7	
0.3 decrease (2) _c	0.6	0.7	

Table 2. Absorptance variation cases used in the simulation tests

For conductivity, three cases were tested starting from a base value of 0.7 W/m·K (Table 3. Conductivity variation cases used in the simulation tests). One case doubled this conductivity, and another halved it. This process was carried out both under the base absorptance value (0.9), and again under a reduced absorptance of 0.7 to observe how both variables interact. In total, six combinations were simulated, offering insight into how conductivity and surface reflectivity jointly influence pavement temperature profiles.

Conductivity variation cases					
Iteration (Step) Absorptance Conductivity (W/m·K)					
Base (1)	0.9	0.7			
Double (2) _d	0.9	1.4			
Half (2) _e	0.9	0.35			
Base with 0.7 absorptance (2) _f	0.7	0.7			
Double with 0.7 absorptance (2) _f	0.7	1.4			
Half with 0.7 absorptance (2) _f	0.7	0.35			

Table 3. Conductivity variation cases used in the simulation tests

These test simulations confirmed the viability of the tool to simulate realistic and varied pavement scenarios. They also provided reference thresholds that will support the analysis and validation stages in the upcoming demonstration phases of the project (Tasks 11.2 and 15.2).

5.1.3. URBAN SIMULATION TESTS

As mentioned earlier, the demo site has not been defined during this development period. Therefore, a **hypothetical site of a representative section** of a Barcelona street was modelled for testing purposes. Based on this urban-scale environment, two buildings were modelled using **CYPETHERM's 3D editing capabilities** within the "3D model" tab. These buildings represent **envelope constructions** and were created in alignment with the pavement zone geometry used in the first part of the workflow (Steps 1 and 2).

The urban environment (Figure 11) consisted of **two similar buildings** of three storeys each, measuring (20 m) x (20 m) in plan and standing opposite one another. They were separated by a **10-m-wide street**, which represents the **pavement section previously analysed**. The street was oriented along a **north-south axis** to maximise its exposure to solar radiation during the day. This simplified representation allowed for the testing of thermal behaviour without the need for precise real-case geometries, which was not the objective of this demonstrative task. The focus remained on **comparing variations between simulations**, which only required a consistent geometry, not one that



replicates a real street.

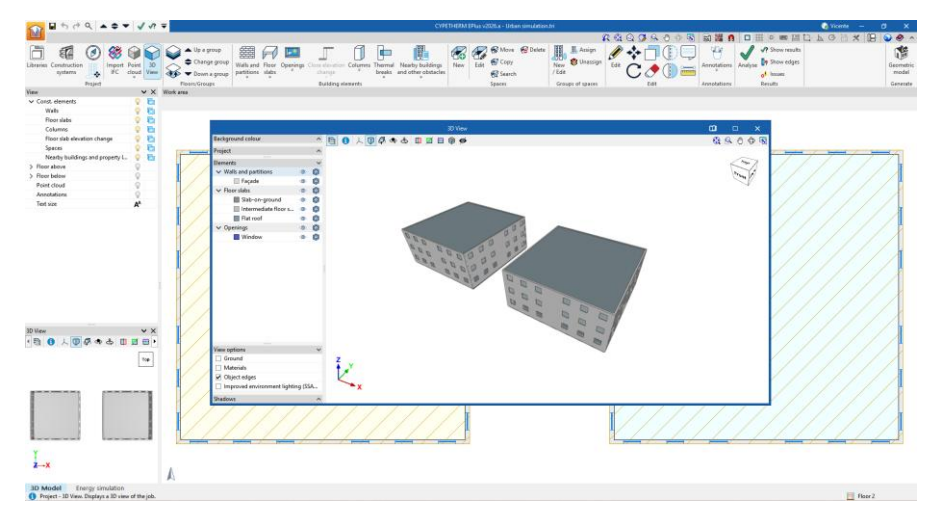


Figure 11. Urban environment created using CYPETHERM's 3D model tab (CREDITS: CYPE)

Within the 'Energy simulation' tab, the **construction elements** for each building (Figure 12) were assigned material properties sourced from CYPETHERM's internal material catalogue. For example, the walls were composed of typical commercial multilayer solutions that included masonry, insulation, and finishing layers, for complying with national regulations. These values, representative of standard buildings in Mediterranean climates, ensured that the simulation results would remain consistent with real-world performance patterns.

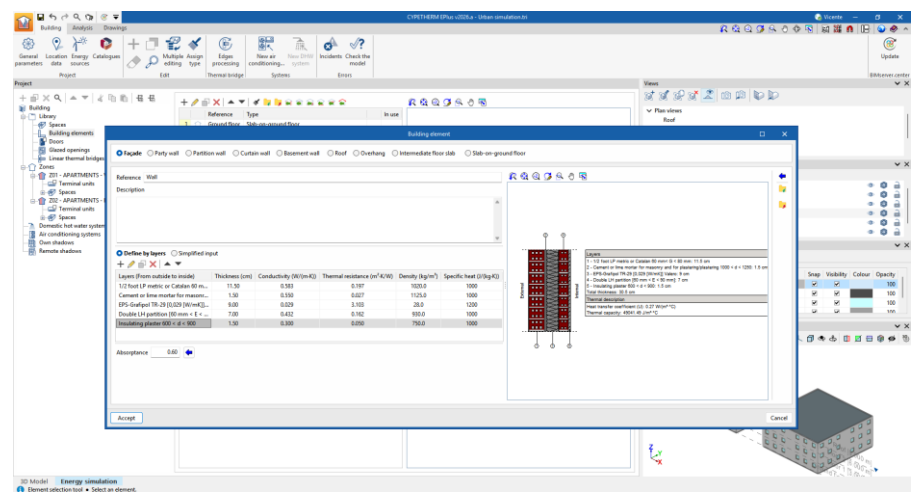


Figure 12. Building envelope layers defined for the simulation (CREDITS: CYPE)

To complete the simulation conditions, the internal operational settings for the building zones were configured to reflect standard comfort thresholds typically used in residential environments. As shown in Figure 13, the interior spaces were classified as "Habitable" and assigned natural ventilation and air infiltration settings. Heating and cooling comfort thresholds were configured, with indoor temperature setpoints established at 20 °C for heating and 25 °C for cooling. These values allowed for the simulation of energy demand responses to external temperature changes and were used to evaluate the impact of ambient variations resulting from different pavement solutions.



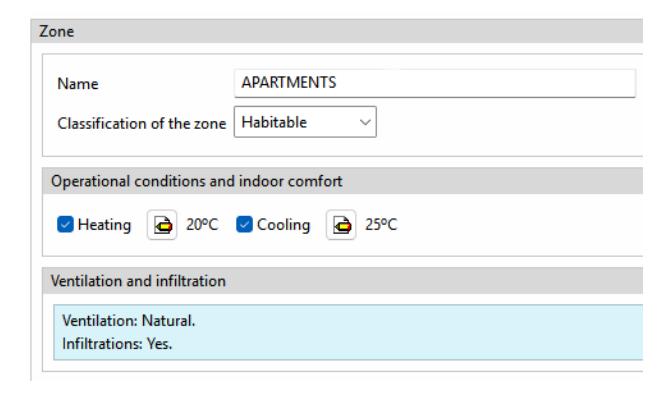


Figure 13. Internal operational settings for the building simulations (CREDITS: CYPE)

With the geometry, material properties, and thermal thresholds in place, the model was prepared for thermal analysis. The first simulation corresponded to **Step 3** of the workflow, representing the existing pavement solution influence on the building environment. The simulation was executed using the **default EPW** file, representing Barcelona's typical climatic data (Figure 14).

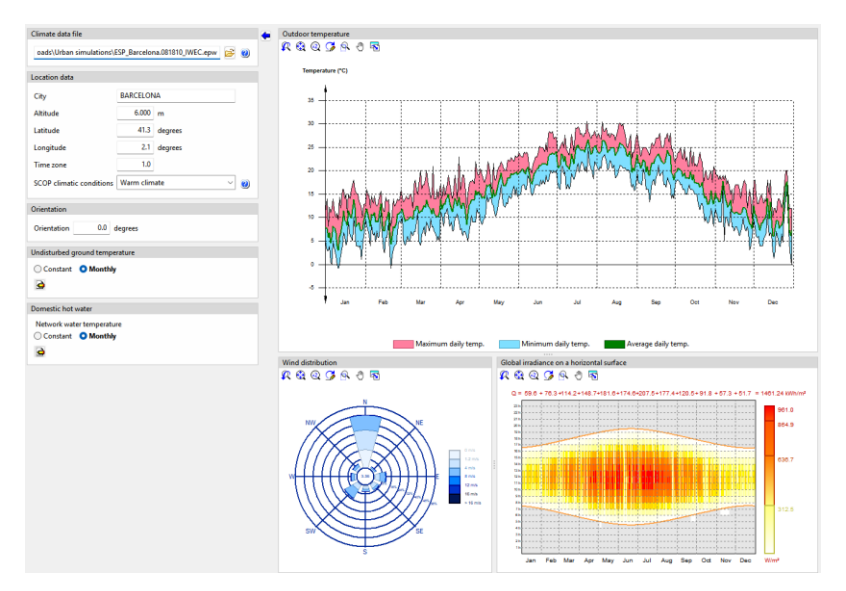


Figure 14. Graphical representation of the EPW file data within CYPETHERM Eplus (CREDITS: CYPE)

Subsequently, to replicate the expected effects of implementing a new pavement solution with modified thermal properties, three additional simulations were conducted (**Step 4** in the workflow). These simulations incorporated altered environmental temperature conditions based on the temperature variations observed in previous pavement simulations. The changes were introduced by editing the EPW file and adjusting ambient temperature values accordingly (Figure 15).



```
*0*0E8*0*0,25.0,17.5,63,100200
                                  )*0E8*0*0,24,17.5,63,100200,1
A7*0E8*0*0,25.2,17.2,61,100100
                                  7*0E8*0*0,24.2,17.2,61,100100
*0*0E8*0*0,26.0,15.4,52,100200
                                  )*0E8*0*0,25,15.4,52,100200,8
*0*0E8*0*0,26.8,13.2,43,100200
                                  )*0E8*0*0,25.8,13.2,43,100200
A7*0E8*0*0 27.6 10.8,35,100200
                                  7*0E8*0*0 26.6 10.8,35,100200
*0*0E8*0*0,25.6,10.1,38,100400
                                  )*0E8*0*0,24.6,10.1,38,100400
*0*0E8*0*0,23.6,9.3,40,100500,
                                  )*0E8*0*0,22.6,9.3,40,100500,
A7*0E8*0*0,21.6,8.4,43,100700,0
                                  /*0E8*0*0,20.6,8.4,43,100700,
*0*0E8*0*0,21.0,7.8,42,100800,6
                                  )*0E8*0*0,20,7.8,42,100800,0,
```

Figure 15. EPW file modification for 1 °C decrease (CREDITS: CYPE)

The ambient temperature was **decreased by 1 °C, 2 °C, and 3 °C** in the first three iterations, while in the fourth modification it was **increased by 1 °C**, as a reference value (Table 4). These reductions were selected to emulate plausible microclimatic changes resulting from varying surface heat emissions, as estimated in steps 1 and 2 of the workflow. The simulations aimed to assess the impact of these changes on building energy demand and indoor conditions. These results are detailed in section 6.1.

EPW ambient temperature variation cases			
Iteration (Step) Ambient temperature variation (°C			
Base (3)	-		
1st modification (4) _a) _a -1 °C		
2 nd modification (4) _b	-2 °C		
3 rd modification (4) _c	-3 ℃		
4 th modification (4) _d	+1 °C		

Table 4. EPW ambient temperature variations cases used for urban simulations

5.2. DATA-DRIVEN DIGITAL TOOL

The work carried out during the second phase of the development of the data-driven digital tool, corresponding to task 10.3, has focused mainly in two points: i) comparison of the automatically generated models against models built manually, and ii) definition and calculation of the final KPI of the digital tool. In addition, the application of the engine developed in task 4.3 to a different dataset has led to the fine-tuning of the previous design of the automatic RC model generator.

5.2.1. MANUAL CALIBRATION OF RC MODELS

The manual calibration of the RC models is done using the Continuous Time Stochastic Modelling for R (CTSMR) package (Vetter et al.). CTSMR is a tool for estimating embedded parameters in a continuous time stochastic state space model. It has been developed at Danish Technical University (DTU) Compute over many years. The package CTSMR provides a new scripting interface through the statistical language R. CTSMR estimates model parameters by minimizing the negative log-likelihood using the quasi-Newton optimizer.

In an incremental approach, models of different complexity are built, from 1-state models to n-state models, where n is the complexity of the optimal model. In a similar manner as in the automated calibration engine of the digital too, the optimal model is defined as the model that shows the best BIC value, i.e., the smallest model able to describe the main aspects of a given dataset. This guarantees the equilibrium between complexity and accuracy.



5.2.2. KPI OF THE DATA-DRIVEN DIGITAL TOOL

Following the advances done during the first year of the project, the KPI calculated by the digital tool is the operative temperature (T_{OP}) . This parameter is a measure used to describe the overall thermal comfort of a space, combining the effects of:

- Air temperature, i.e., the temperature of the air surrounding a person.
- Mean radiant temperature, that is the average temperature of surrounding surfaces that emit or absorb thermal radiation.

And it can be defined as seen in Eq. (3):

$$T_{OP} = \frac{T_R + (T_A \cdot \sqrt{10 \cdot v})}{1 + \sqrt{10 \cdot v}}$$
(3)

where T_R [°C] is the radiant temperature, T_A [°C] the ambient temperature, and v [m/s] the wind speed. However, in contrast to what would be the case if the radiant temperature were calculated inside a building, its calculation is not straightforward when used outdoor.

Radiant temperature is a comprehensive measure of the thermal environment, capturing the cumulative effect of surrounding surface temperatures and radiation sources, including both shortwave (solar) and longwave (thermal) radiation, on the net heat exchange between an individual and their surroundings. It is defined as the uniform temperature of a hypothetical enclosure that would result in the same amount of radiant heat gain or loss as the actual, non-uniform environment. In outdoor settings, the primary factors influencing radiant temperature are the surface temperature of surrounding surfaces and the sky temperature. From the perspective of integrating this variable into the digital tool, the surface temperature can be directly obtained as an output from the data-driven model. However, an auxiliary model is required to estimate the sky temperature.

Sky temperature (T_{sky}) represents the effective radiant temperature of the sky, equivalent to the temperature of a blackbody emitting the same amount of longwave infrared radiation as the actual sky. When longwave solar radiation is available, sky temperature can be calculated using the following method (Zhang et al.):

$$T_{sky} = \left(\frac{Q_{LWD}}{s}\right)^{1/4} \tag{4}$$

Where σ [W/m²K⁴] is the Stefan-Boltzmann constant and Q_{LWD} [W/m²] the measured longwave radiation. However, this calculation is not usually possible as devices that can measure longwave radiation are expensive and are not normally installed. To address this limitation, several studies have been published (Evangelisti et al.) to provide alternative methods for estimating sky temperature using more commonly available parameters.

Models used to calculate sky temperature can be broadly categorized into two groups: i) direct models and ii) detailed models. Direct models, e.g., the ones based on ISO 13790 ('ISO 13790'), provide a simplified calculation of the T_{sky} parameter based on T_A values. Table 5. Direct models according to ISO 13790 includes the three different correlations that can be used for this calculation, depending on the location of the measurement.

Correlation	Site	
$T_{sky} = T_A - 11$	Temperate areas	
$T_{sky} = T_A - 9$	Sub-polar areas	
$T_{sky} = T_A - 13$	Tropical areas	

Table 5. Direct models according to ISO 13790





In contrast, detailed models are more complex and require detailed information as input to establish the correlations. These models involve a two-step process, where sky emissivity is first calculated, followed by the calculation of sky temperature. The sky temperature can be subsequently calculated using the relationship presented in Eq. (5).

$$Q_{LWD} = s \cdot T_{skv}^{4} = \varepsilon_{skv} \cdot s \cdot T_{amb}^{4} \tag{5}$$

Where Q_{LWD} [W/m²] is the measured longwave radiation, σ [W/m²K⁴] the Stefan-Boltzmann constant, and ε_{skv} [-] the sky emissivity.

Table 6 includes a summary of the most used detailed models to calculate clear sky emissivity. Given the urban island heat effect is most pronounced on sunny days with minimal cloud cover, it is assumed that clear sky emissivity can be used to simulate the worst-case scenario when calculating radiant temperature. This approach allows for the simplification of the calculation by disregarding the effect of clouds on clear sky emissivity. After comparing and evaluating the various available models, considering factors such as their validation through real-world data, the detailed model developed by Prata has been selected for calculating clear sky emissivity within the digital tool.

Reference	Date	Correlation
(Bliss)	1961	$\varepsilon_{sky} = 0.8004 + 0.00396T_{dp}$
(Staley and Jurica)	1972	$\varepsilon_{sky} = 0.67 P_v^{0.08}$
(Brutsaert)	1975	$\varepsilon_{sky} = 1.24(P_v/T_A)^{1/7}$
(Prata)	1996	$\varepsilon_{sky} = 1 - (1 + \varphi)e^{-\sqrt{1.2 + 3\varphi}}, \varphi = 46.5(P_v/T_A)$
		$\varepsilon_{sky} = 1 - e^{(-1.66\tau)}, \tau = 2.232 - 1.875 \left(\frac{T_A}{273.15}\right) + 0.7356\sqrt{18.6(P_v/T_A)}$
(Dilley and O'brien)	1998	$\varepsilon_{sky} = \frac{1}{s \cdot T_A^4} \left[59.38 + 113.7 \left(\frac{T_A}{273.15} \right)^6 + 96.96 \sqrt{18.6(P_v/T_A)} \right]$

Table 6. Detailed clear sky models, where ε sky [-] is the sky emissivity, Tdp [°C] the dew point temperature, TA [°C] ambient temperature, and Pv [mb] the vapor pressure.

Once sky temperature is calculated, through the obtention of the sky emissivity value, radiant temperature is calculated as shown in Eq. (6):

$$T_R = \left[\frac{S_{abs}}{\varepsilon \cdot s \cdot f_{cl}} + s \cdot \left(f_{sky} \cdot T_{sky}^4 + \left(1 - f_{sky}\right) \cdot T_{surf}^4\right)\right]^{1/4}$$
(6)

Where S_{abs} [W/m²] is the absorbed shortwave radiation, ε [\approx 0.95] the emissivity of clothing, σ [W/m²K⁴] is the Stefan-Boltzmann constant, f_{cl} [\approx 0.7] is the clothing form factor, f_{sky} is the sky view factor [\approx 0.4 in urban environment], T_{sky} [K] is the sky temperature, and T_{surf} [K] is the surface temperature.

The actual validation of the proposed radiant temperature calculation will be conducted in Task 11.2, utilizing the radiant temperature data monitored at the Spanish demo site. In contrast, the results section for the data-driven digital tool will focus on validating the performance of the designed automated RC model generator engine, specifically assessing its ability to accurately generate models for predicting surface temperature.



6. RESULTS

6.1. PHYSICS-BASED MODELLING TOOL

As part of the preparation for applying the new functionalities of the physics-based modelling tool in the Spanish demo case, a series of tests were conducted to ensure its reliability and relevance. By using the proposed **workflow and iterations** described in section 5.1, simulations were carried out to evaluate the behaviour of pavements and surrounding buildings, particularly analysing isolated and combined thermal interactions, as well as the influence of projected shadows of adjacent buildings in the pavement. These tests helped to anticipate the behaviour of the proposed pavement solution and the overall impact of urban structures on microclimatic dynamics, in the context of the urban heat island (UHI) phenomenon.

To analyse these simulations, the **KPIs defined in D4.3** were used to assess the tool consistency and comparative capabilities. These included surface temperatures, heat transfer rate through pavement, heating and cooling demands of adjacent buildings, and indoor operative temperatures. Also, by comparing the results of different material configurations and environmental inputs, the tool outputs served to **provide reference values for future validation** using real-world data from the Spanish demo case (Tasks 11.2 and 15.2).

As a remark, it is important to mention that the EPW file used for the simulations is based on historical average conditions obtained from standardised measured data from Barcelona's airport zone. These values do not necessarily reflect the exact current or future climate reality, particularly considering the accelerating effects on global warming, which have led to abrupt, more frequent, and intense heat waves and other extreme weather events. However, due to the unpredictability and variability of these phenomena, there is current no standardised method to incorporate such conditions consistently into the simulations needs. Therefore, the results on the physics-based modelling tool should be interpreted just as references and as representative under historical conditions, rather than as projections under future climate stress scenarios.

6.1.1. SURFACE TEMPERATURE

Surface temperature was identified as one of the most sensitive and direct indicators of pavement performance. Based on the iterations described in Section 5.1, two series of tests were conducted to assess the effect of changing key material properties on this KPI: absorptance and thermal conductivity.

The analysis focused on peak surface temperatures observed in the simulations. Based on the EPW climate data file for Barcelona, the highest external temperature of the year occurs on **July 7**th **at 13:00**. However, due to the materials thermal inertia, the pavement surface temperatures reached their peak **at 14:00**, which was adopted as the reference time for the comparative analysis of all iterations.

A first set of simulations explored the impact of modifying the asphalt layer absorptance, ranging from 0.9 (baseline) to 0.6 with 0.1 steps. The corresponding surface temperature curves show a consistent pattern as shown in Figure 16: all variations follow a similar diurnal evolution, with differences appearing progressively from mid-morning onwards. From approximately 10:00 to 17:00, the differences between curves become more evident, indicating that absorptance influences heat accumulation during the hours of highest solar radiation. While early morning and late-night temperatures remain largely unaffected, the curve associated with the base absorptance (0.9) rises more steeply and peaks at the highest value, suggesting that darker surfaces retain and absorb significantly more energy during the day.



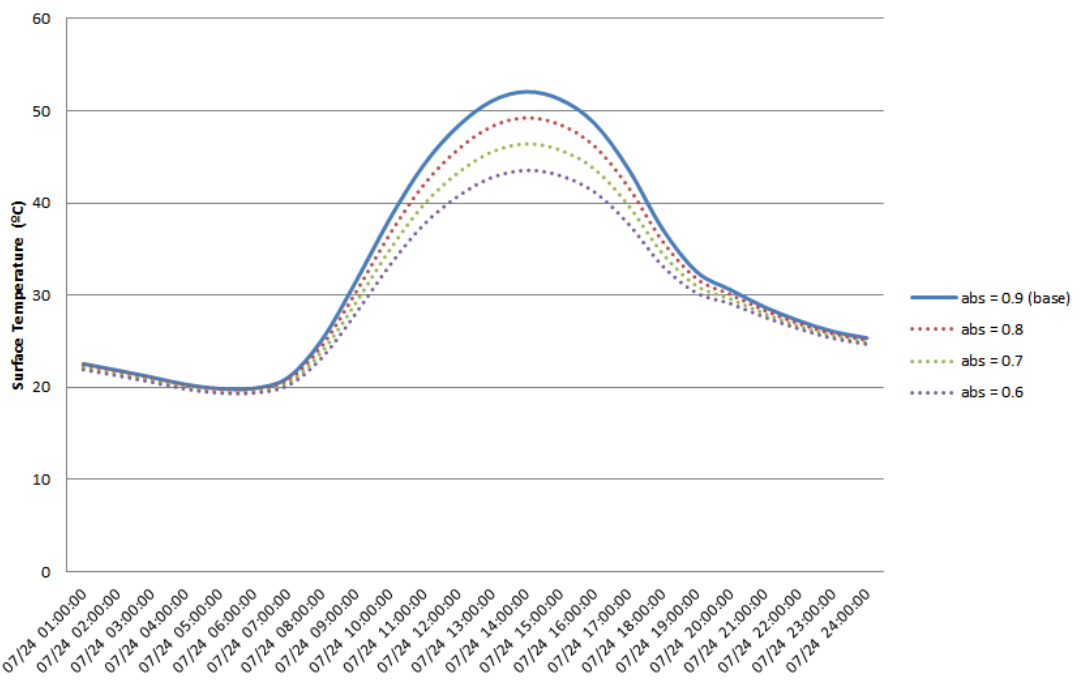


Figure 16. Hourly surface temperature variation by absorptance iteration (CREDITS: CYPE).

When analysing peak temperatures (Table 7. Peak surface temperature results for absorptance iterations; Figure 16. Hourly surface temperature variation by absorptance iteration (CREDITS: CYPE).), results showed a clear linear relationship between lower absorptance values and surface temperature reduction. For every 0.1 decrease in absorptance, the peak surface temperature was reduced by approximately 2.90 °C, with the maximum difference between the base and lowest case reaching 8.53 °C.

Peak surface temperature results for Absorptance iterations						
Iteration (Step) Absorptance Conductivity (W/m·K) Peak surface (W/m·K) temperature (°C)						
Base (1)	0.9 0.7 52.07					
0.1 decrease (2) _a	e (2) _a 0.8 0.7 49.24					
0.2 decrease (2) _b 0.7 0.7 46.40						
0.3 decrease (2) _c 0.6 0.7 43.54						

Table 7. Peak surface temperature results for absorptance iterations

This trend demonstrates that more reflective surfaces can contribute significantly to reduce surface overheating. Notably, even **modest improvements in albedo** (e.g., increasing it from 0.1 to 0.2) already show a **measurable cooling effect**, which could be particularly useful for designing mitigation strategies in urban areas prone to extreme heat.

It is important to mention that the timing of the peak remains consistent across all iterations—occurring at 14:00—but the intensity of the peak is directly mitigated by the absorptance reduction. This confirms that modifying surface colour or finish (to lower absorptivity) is an effective passive strategy to limit surface overheating, particularly during critical summer hours.

A second set of tests focused on modifying the thermal conductivity of the top pavement layer. Starting from a base value of 0.7 W/m·K, the material conductivity was halved and doubled to



examine both extremes. The **results were more subtle** compared to absorptance. Doubling conductivity from 0.7 to 1.4 reduced the peak surface temperature by approximately 1.05 °C, likely due to improved heat dissipation into the deeper layers. On the other hand, halving conductivity to 0.35 W/m·K increased surface temperature by 1.36 °C, indicating greater heat retention near the surface.

When analysing the shape of the curves in Figure 17, it is clear that the conductivity variations influence the slope of the rise and fall of the temperature profile. The lower conductivity case shows a slightly delayed and more prolonged cooling phase in the afternoon, suggesting **thermal inertia** effects that keep the pavement warmer for longer. In contrast, the high-conductivity scenario cools down more rapidly after the peak.

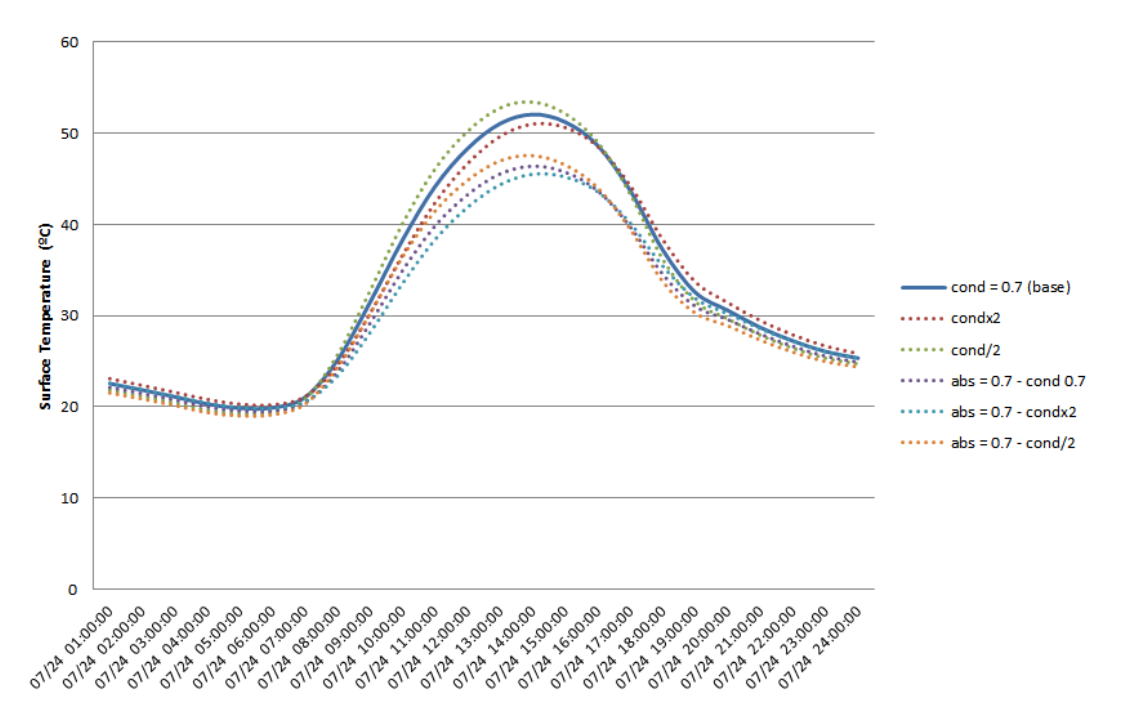


Figure 17. Hourly surface temperature variation by conductivity and hybrid iterations (CREDITS: CYPE)

Regarding the interaction effects between absorptance and conductivity (Table 8), when combining lower absorptance (0.7) with conductivity variations, the results showed that **absorptance remained** the dominant factor in determining surface temperature. However, conductivity still introduced noticeable variations of temperature within the same absorptance group. For instance, under a 0.7 absorptance setting, doubling conductivity reduced peak temperature by 0.89 °C, while halving it raised it about 1.14 °C.

The temperature profiles in these combined cases reveal smoother and less extreme curves than those based on high-absorptance materials. Moreover, the simultaneous adjustment of both properties can be used as a balancing mechanism: even if surface colour cannot be altered, conductivity tuning can still offer performance gains. In these cases, thermal inertia behaviour appears more stabilised, with narrower peaks and earlier cooling transitions observable from around 15:30 onward.

Peak surface temperature results for Conductivity iterations			
Iteration (Step)	Absorptance	Conductivity (W/m·K)	Peak surface Temperature (°C)



Base (1)	0.9	0.7	52.07
Double (2) _d	0.9	1.4	51.02
Half (2) _e	0.9	0.35	53.43
Base with 0.7 absorptance (2) _f	0.7	0.7	46.40
Double with 0.7 absorptance (2) _f	0.7	1.4	45.51
Half with 0.7 absorptance (2) _f	0.7	0.35	47.54

Table 8. Peak surface temperature results for conductivity iterations

The simulation outputs confirm the capability of the tool not only to simulate precise surface temperatures under variable input conditions, but also to capture time-based behaviours associated with material property interaction, an essential feature for accurate urban thermal performance modelling.

6.1.2. HEAT TRANSFER RATE THROUGH PAVEMENT

The second KPI analysed was the heat transfer rate through the pavement layers. This indicator helps quantify how much energy penetrates or is released from the pavement over time and is therefore a key factor in understanding how thermal properties affect not only the surface temperature but also subsurface and environmental thermal exchanges.

The analysis (Figure 18) shows that the maximum heat transfer rate consistently occurred around 11:00 a.m., earlier than the surface temperature peak at 14:00 observed in the previous section. This is likely explained by the time lag between incoming solar radiation and the surface thermal response. As the pavement absorbs energy in the morning, the heat wave begins to propagate through the material layers, reaching a peak in heat flux before the surface itself reaches its maximum temperature. This behaviour depicts the effect of thermal inertia and material depth on heat propagation dynamics.

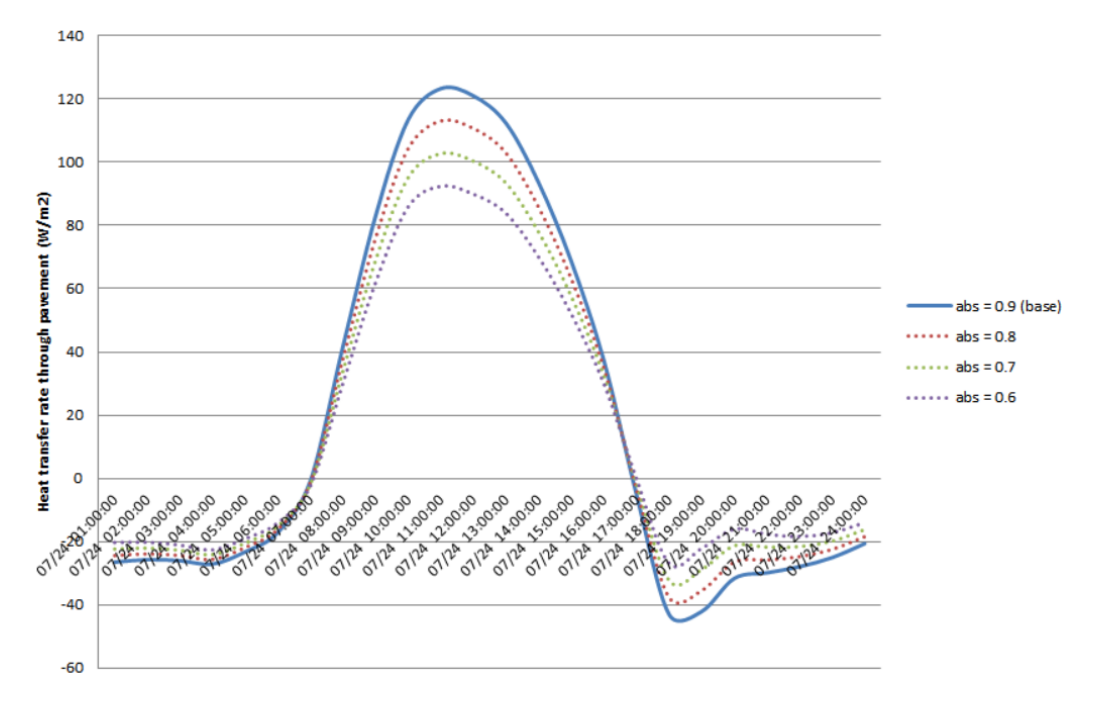


Figure 18. Hourly heat transfer rate through pavement by absorptance iterations (CREDITS: CYPE)



The first iterations were done by varying different absorptance values. While all cases follow the same diurnal pattern, higher absorptance (e.g., 0.9) yields significantly higher peaks and a steeper increase in the morning hours. Lower absorptance flattens the curve and reduces both the intensity and duration of daytime heat transfer. By 14:00, all curves begin to converge, and the differences narrow significantly. This confirms that absorptance has its strongest influence during peak solar radiation hours, aligning with earlier observations on surface temperature.

These behaviours were also reflected in the peak values, depicted in Table 9. As absorptance decreased from 0.9 to 0.6, the peak heat transfer rate dropped from 123.31 W/m² to 92.40 W/m², which is a 25% decrease. On average, each 0.1 reduction in absorptance led to approximately 10 W/m² reduction in peak energy flux. This further reinforces the idea that surface colour or treatment significantly affects not only surface heat retention but also how much energy is transmitted into the structure and surrounding environment.

Peak heat transfer rate through pavement results for Absorptance iterations					
Iteration (Step) Absorptance Conductivity (W/m·K) Heat transfer rate through the stransfer rate thr					
Base (1)	0.9	0.7	123.31		
0.1 decrease (2) _a	0.8	0.7	113.05		
0.2 decrease (2) _b	0.7	0.7	102.74		
0.3 decrease (2) _c	0.6	0.7	92.40		

Table 9. Peak heat transfer rate through pavement results by absorptance iterations

The second set of iterations represents the results of the conductivity variation tests, both under the base absorptance (0.9) and a reduced value (0.7). The most visible effect of higher conductivity (1.4 W/m·K) is the **sharper and more intense curve**, reaching its peak earlier and decreasing more rapidly, even dipping below zero after sunset (Figure 19). In contrast, lower conductivity values yield **flatter**, **wider curves** that prolong energy retention and delay the pavement's release of stored heat. These shifts are especially notable during early evening hours, where the high-conductivity case shows significant negative flux values—indicating energy loss from the pavement back to the air or surrounding structures.



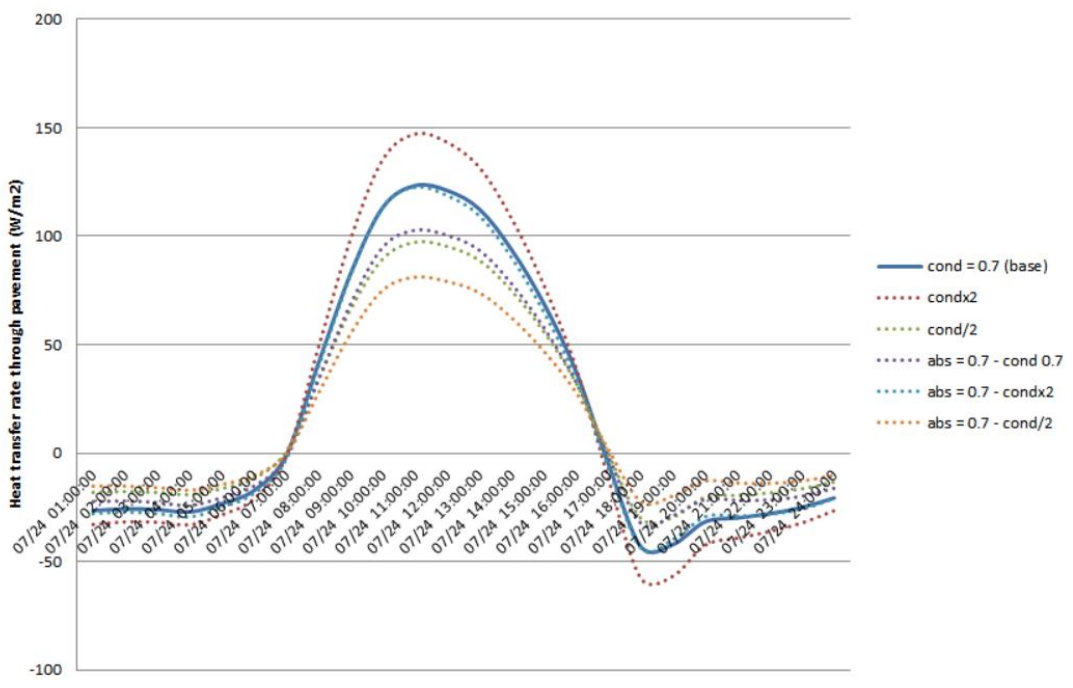


Figure 19. Hourly heat transfer rate through pavement by conductivity and hybrid iterations (CREDITS: CYPE)

Moreover, when conductivity was modified under a fixed absorptance of 0.7 (Table 10), the maximum fluxes were lower across the board, confirming that absorptance still exerts the dominant influence. For instance, at 0.7 absorptance, increasing conductivity doubled the flux from 81.10 W/m² (low conductivity) to 122.53 W/m² (high conductivity). This clearly shows that combining moderate absorptance with conductivity can either amplify or suppress heat exchange, depending on the design objectives: thermal comfort, cooling loads, or climate adaptation.

These observations validate the physics-based tool ability to simulate detailed subsurface thermal interactions. They also illustrate how the variation of a few material parameters can influence the thermal footprint of pavement solutions at both surface and structural levels

Peak heat transfer rate through pavement results for Conductivity iterations				
Iteration (Step)	Absorptance Conductivity Heat transfer rate thro			
Base (1)	0.9	0.7	123.31	
Double (2) _d	0.9	1.4	147.10	
Half (2) _e	0.9	0.35	97.22	
Base with 0.7 absorptance (2) _f	0.7	0.7	102.74	
Double with 0.7 absorptance (2) _f	0.7	1.4	122.53	
Half with 0.7 absorptance (2) _f	0.7	0.35	81.10	

Table 10. Peak heat transfer rate through pavement results for conductivity and hybrid iterations

6.1.3. HEAT EMISSION TO AIR

Even though it was not explicitly declared as a KPI in D4.3, heat emission to air was included in the current evaluation to gain an early understanding of how different pavement configurations may



contribute to the **Urban Heat Island (UHI)** effect. This parameter reflects the amount of thermal radiation that escapes from the pavement into the surrounding air and therefore plays a key role in shaping local microclimates, especially during periods of prolonged solar exposure.

Figure 20 shows the hourly heat emission to air under different absorptance conditions. The shape of the curves closely mirrors that of surface temperature evolution, peaking at **14:00**, which corresponds with the moment of highest pavement surface temperature. This delay, relative to earlier heat transfer peaks (seen around 11:00), again reflects **thermal inertia**. In this case, the accumulated heat reaching the surface before being radiated back to the atmosphere.

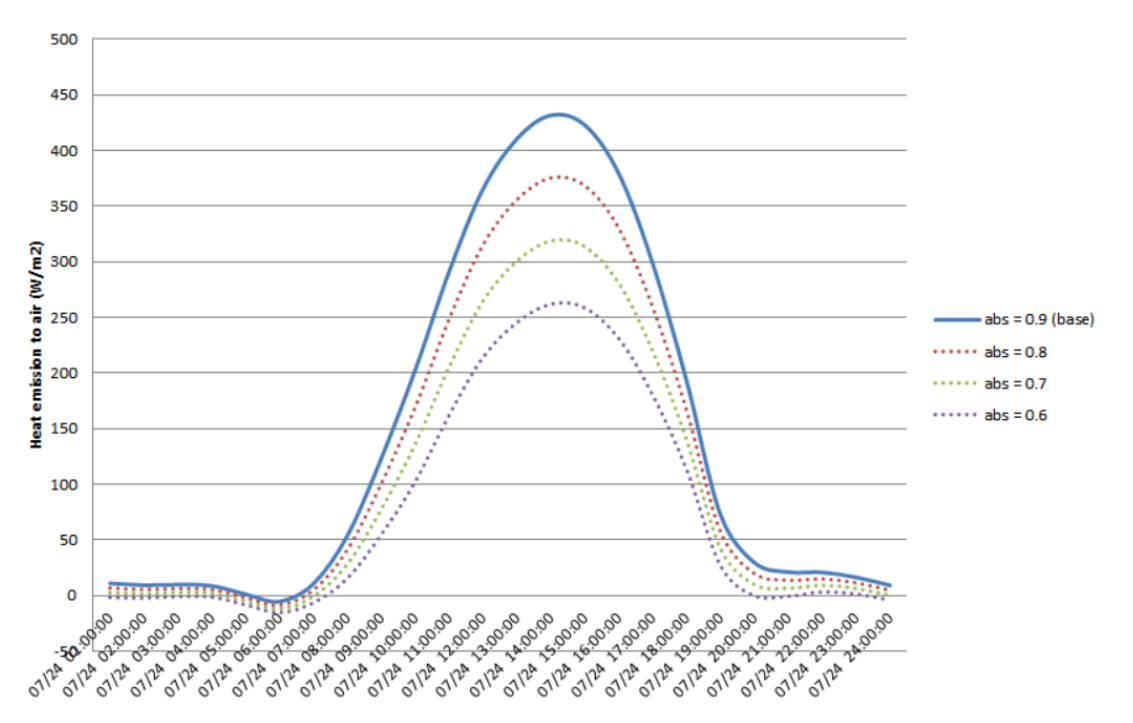


Figure 20: Hourly heat emission to air by absorptance iterations (CREDITS: CYPE)

The variation across iterations is consistent and follows a clear gradient: higher absorptance leads to higher emissions. Specifically, the **curve for the base case (0.9)** peaks sharply and returns to predawn levels more slowly, indicating a longer period of high-energy exchange. On the other hand, the lowest absorptance case (0.6) results in a much smoother curve, peaking lower and dissipating earlier, suggesting reduced heat exchange with the ambient air. This indicates that **lower absorptance pavements may mitigate UHI intensity** by reducing the radiative heat load imposed on the urban atmosphere.

These observations are confirmed by the peak values shown in Table 11. Peak heat emission to air results for absorptance iterations The base configuration (0.9) reached a maximum emission of 431.53 W/m², while a 0.3 reduction in absorptance brought the value down to 261.99 W/m². This represents a nearly 40% decrease in heat emission, suggesting that minor material property adjustments could significantly affect the surface-to-air thermal exchange. On average, each 0.1 decrease in absorptance yielded a reduction of around 57 W/m² in peak heat emission.

Peak heat emission to air results for Absorptance iterations				
Iteration (Step) Absorptance Conductivity (W/m·K) Heat emission to air (W/m·K) (W/m^2)				
Base (1)	0.9	0.7	431.53	



0.1 decrease (2) _a	0.8	0.7	375.32
0.2 decrease (2) _b	0.7	0.7	318.81
0.3 decrease (2) _c	0.6	0.7	261.99

Table 11. Peak heat emission to air results for absorptance iterations

The second set of iterations shows the behaviour of this parameter (Figure 21) under variations in conductivity and hybrid scenarios (e.g. combining with absorptivity variations). When thermal conductivity was doubled, the emission curve became narrower and taller, reflecting a rapid intake and subsequent release of heat. On the contrary, halving the conductivity led to broader and lower curves, suggesting a slower and more gradual thermal cycle. Notably, the halved conductivity case (cond/2) exhibits a peak even higher than the base case, likely because of reduced thermal dissipation to lower layers, forcing more energy to be emitted upward.

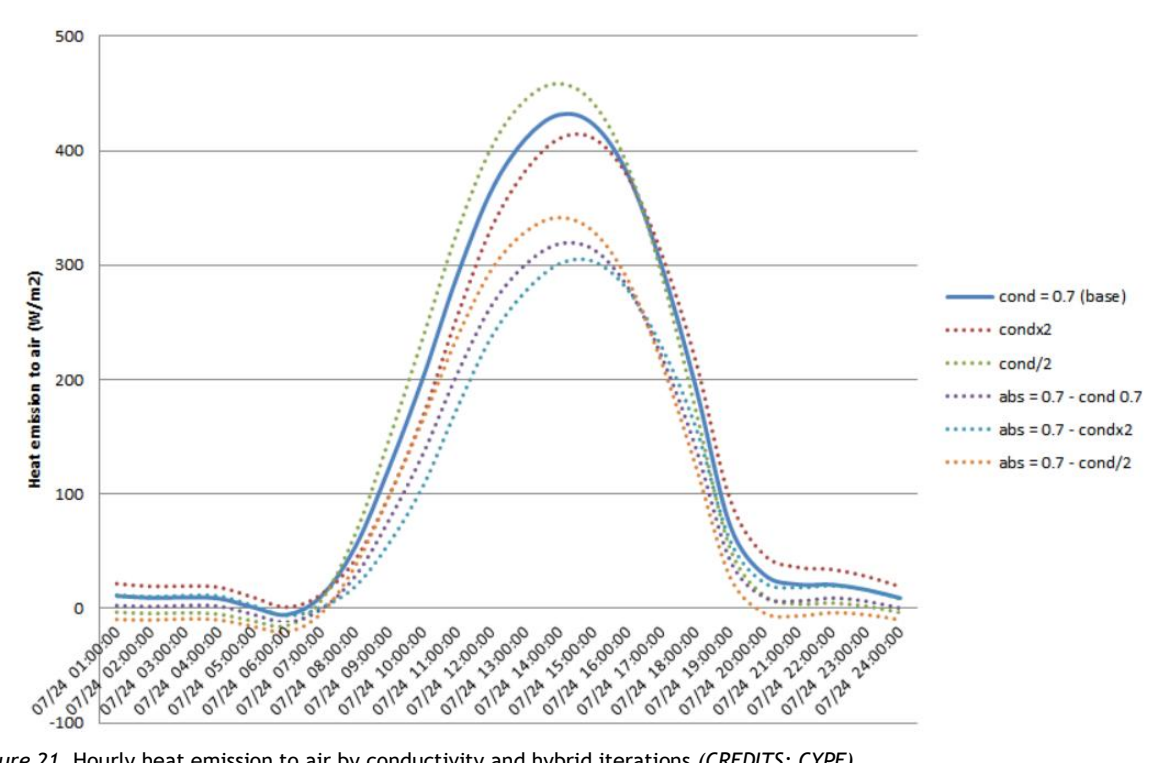


Figure 21. Hourly heat emission to air by conductivity and hybrid iterations (CREDITS: CYPE).

It is also interesting to point out that under the hybrid condition of absorptance = 0.7, higher conductivity still led to flatter curves, but they remained consistently below the base case. This interaction implies that even if conductivity amplifies vertical heat flow, the dominant factor in surface emission remains absorptance. The flatter and lower the curve, the less thermal radiation reaches the surrounding air, indicating a cooler and more stable microclimate.

Peak heat emission to air results for Conductivity iterations					
Iteration (Step) Absorptance Conductivity $(W/m \cdot K)$ Heat emission to air $(W/m \cdot K)$ (W/m^2)					
Base (1) 0.9 0.7 431.53					
Double (2) _d 0.9 1.4 410.71					
Half (2) _e 0.9 0.35 458.56					



Base with 0.7 absorptance (2) _f	0.7	0.7	318.81
Double with 0.7 absorptance (2) _f	0.7	1.4	301.26
Half with 0.7 absorptance (2) _f	0.7	0.35	341.55

Table 12. Peak heat emission to air results by conductivity and hybrid iterations

The peak values support this interpretation, as shown in Table 12. Doubling conductivity under the base absorptance meant a heat emission of 410.71 W/m²; while halving it produced the highest recorded value: 458.56 W/m². This reinforces the idea that reduced conductivity traps heat near the surface, therefore increasing surface temperatures and outgoing radiation. However, under an absorptance of 0.7, emissions dropped considerably. The highest emission in this case was 341.55 W/m² (at low conductivity), while the lowest was 301.26 W/m² (at high conductivity). This suggests that a thoughtful pairing of materials with moderate absorptance and high conductivity could suppress overall energy re-emission and contribute to better thermal regulation in urban settings.

From a broader perspective, these results show how material properties not only affect internal heat transfer within the pavement but also have a direct influence on the **thermal energy released into the urban atmosphere**. Over large areas and extended periods, these differences may translate into measurable variations in local air temperatures. For instance, a reduction of 100 to 150 W/m² in radiated energy per square metre could substantially reduce ambient heat loads during summer peaks. In future stages of the project, these outputs may serve as early indicators for assessing the potential cooling benefits of alternative pavement strategies in mitigating the UHI effect.

6.1.4. COOLING AND HEATING DEMAND OF ADJACENT BUILDINGS

To assess the potential urban-scale impacts of pavement material changes on indoor energy performance, cooling and heating demand indicators were evaluated for adjacent buildings in accordance with the definitions established in D4.3. While the actual changes in ambient temperature resulting from new pavement solutions are still unknown and will require future validation, the purpose of this analysis was to simulate hypothetical variations and evaluate their influence on building thermal behaviour. This approach allows for an early understanding of how surface-level microclimatic interventions could potentially influence surrounding energy performance and occupant comfort.

As summarised in Table 13, the base scenario representing the current situation shows a cooling demand of 18.04 kWh/m²·year and a heating demand of 8.59 kWh/m²·year. When ambient temperature is hypothetically reduced by 1 °C, cooling demand decreases to 15.00 kWh/m²·year while heating demand increases to 11.52 kWh/m²·year. These trends intensify as the ambient temperature continues to drop: at -2 °C, cooling demand falls to 12.16 kWh/m²·year, while heating demand rises to 14.84 kWh/m²·year. The greatest variation occurs at -3 °C, where cooling drops by almost half of the base value to 9.55 kWh/m²·year, but heating demand more than doubles to 18.46 kWh/m²·year.

Cooling and heating demand results for EPW file variations					
Iteration (Step) Ambient temperature variation (°C) Cooling demand Heating (kWh/m²·year) (kWh/m²·year)					
Base (3)	-	18.04	8.59		
1st modification (4) _a	-1 °C	15.00	11.52		
2 nd modification (4) _b	-2 °C	12.16	14.84		



3 rd modification (4) _c	-3 °C	9.55	18.46
4 th modification (4) _d	+1 °C	21.28	6.08

Table 13. EPW ambient temperature variations cases used for urban simulations

On the contrary, when ambient temperature is **increased by 1 °C** (simulating a case where the pavement absorbs and releases more heat into the surroundings), **cooling demand rises** to 21.28 kWh/m^2 ·year while **heating demand drops** to 6.08 kWh/m^2 ·year.

These results confirm the anticipated trade-off between cooling and heating requirements: as outdoor temperatures drop, cooling demand decreases while heating requirements rise, and vice versa. From an annual energy demand perspective, the total demand (cooling plus heating) decreases when conditions are closer to thermal comfort thresholds. However, when deviations grow larger, one of the demands compensates the reduction of the other.

The results highlight the potential of targeted pavement design in balancing cooling and heating needs. In warm climates such as Barcelona's, where cooling is typically the dominant load during summer, pavements designed to reduce ambient temperatures by 1-2 °C could mean significant reductions in cooling demand. Notably, this could not necessarily mean an increase of ambient temperature during winter times, which might put the results into perspective. Nevertheless, these must be carefully weighed against the potential increase in heating energy during winter months, particularly in buildings with low thermal inertia or poor envelope insulation.

Although the temperature modifications explored in this test are theoretical and used only for comparative purposes, the observed patterns indicate a **potential correlation between pavement-induced microclimate changes and the energy consumption profile of nearby buildings**. These outcomes reinforce the relevance of including such indicators when assessing the long-term urban impacts of surface material interventions.

6.1.5. INDOOR OPERATIVE TEMPERATURE

According to D4.3, operative indoor temperatures were defined as a key performance indicator to evaluate the comfort conditions inside buildings influenced by the thermal performance of pavements. These temperatures reflect the expected indoor climate resulting from external changes, without directly modelling HVAC (Heating, Ventilation, and Air Conditioning) system outputs. In this context, a lower indoor operative temperature during warm months may indicate better envelope insulation, increased reflectivity, or the effectiveness of passive cooling strategies, whether through envelope optimisation or indirect urban interventions such as more reflective pavements.

As part of the urban simulation process, the results obtained in CYPETHERM EPlus were divided into two categories: maximum comfort temperature and minimum comfort temperature, both of which provide useful insights into the thermal range occupants might experience. Given that the project focuses on UHI mitigation and thermal stress reduction, it was considered relevant to include both sets of results. The maximum temperature series represents the upper limit of indoor comfort (typically influenced by daytime heat gains) while the minimum temperature may be influenced by night-time cooling and indoor heat losses. Analysing both provides a better understanding of how UHI mitigation may improve indoor thermal conditions throughout the day.

For maximum indoor comfort temperatures, there is a consistent seasonal pattern with the peak indoor operative temperatures reached in August (with a base case result of 33.7 °C), and clear, parallel shifts across all EPW scenarios, indicating a stable and predictable indoor response to changes in outdoor temperature. This aligns with expected seasonal climate behaviour, as August typically concentrates the warmest period in Mediterranean climates, particularly in urban environments with high surface accumulation and low wind activity. As shown in Figure 22, all scenario curves followed the same trend, with a consistent downward shift for scenarios with reduced EPW temperatures.



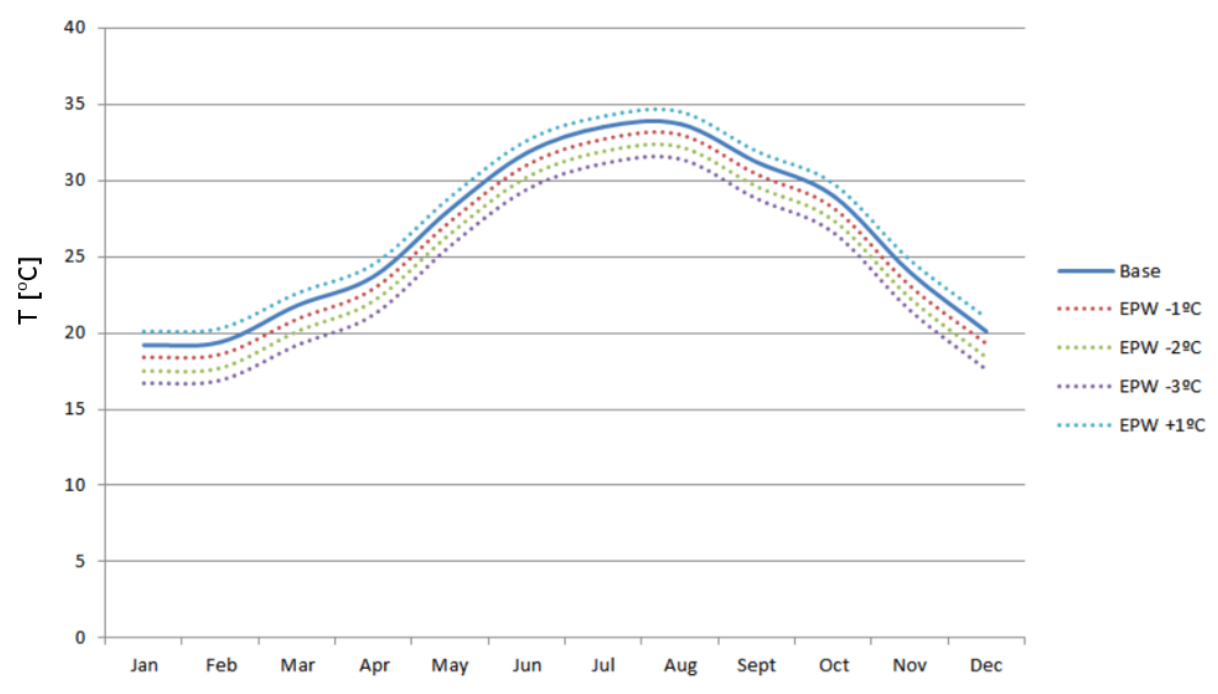


Figure 22. Monthly indoor maximum comfort temperature (CREDITS: CYPE)

A temperature **decrease of 1 °C** in the ambient file led to an approximate **indoor reduction of 0.7 °C** across the entire year, while a -3 °C EPW scenario showed an indoor reduction of more than 2.3 °C in August, going from 33.7 °C to 31.4 °C. This behaviour is further summarised in Table 14. *Peak indoor maximum comfort temperature results for EPW file variations*, which gathers the peak monthly values (reached in August) for each case and shows how indoor operative temperatures evolve under different ambient temperatures.

Peak indoor maximum	or maximum comfort temperature results for EPW file variations				
Iteration (Step)	Ambient temperature variation (°C)	Peak indoor maximum comfort temperature (°C)			
Base (3)	-	33.7			
1st modification (4) _a	-1 °C	33.0			
2 nd modification (4) _b	-2 °C	32.2			
3 rd modification (4) _c	-3 °C	31.4			
4 th modification (4) _d	+1 °C	34.5			

Table 14. Peak indoor maximum comfort temperature results for EPW file variations

Figure 23. Monthly indoor minimum comfort temperature (CREDITS: CYPE) shows that for minimum indoor comfort temperatures the trend is similar, but **peak occurred in July**, reaching 28.8 °C in the base case, and reflecting the influence of accumulated heat gains. This is likely due to **thermal inertia and internal heat gains**, which accumulate gradually throughout the warm season and generate higher indoor base temperatures even during the night. The scenario curves again remained parallel and followed the same consistent pattern seen in the maximum comfort case.



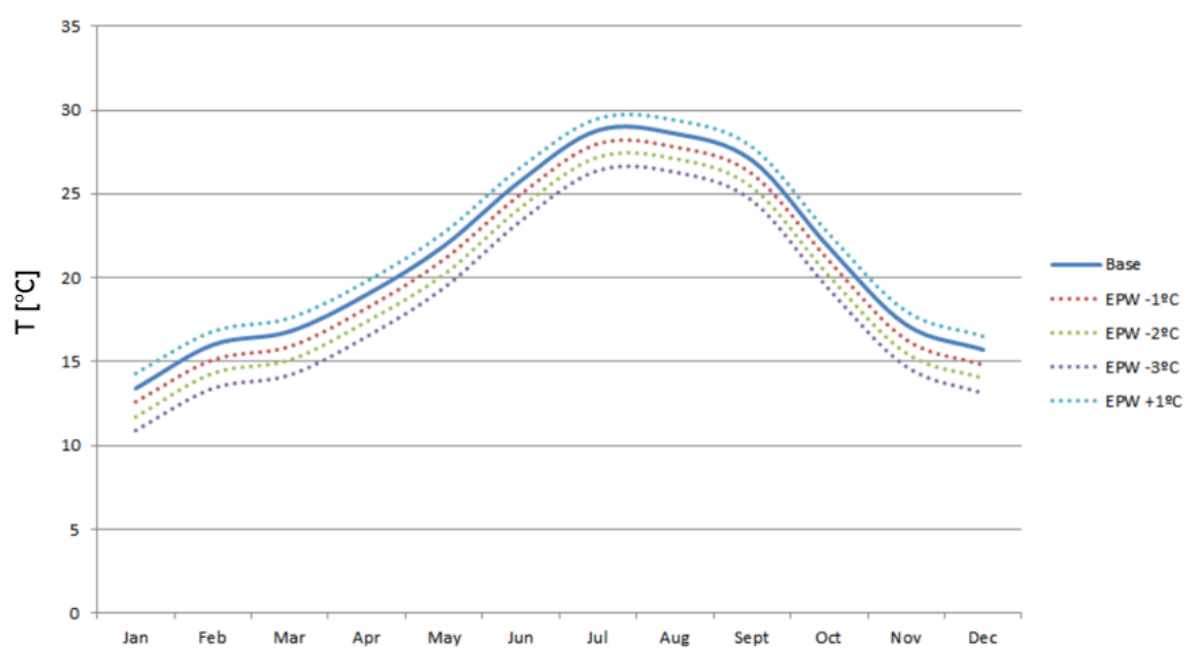


Figure 23. Monthly indoor minimum comfort temperature (CREDITS: CYPE)

The ambient file modified by -1 °C led to a reduction of 0.8 °C in **July's indoor temperature** (28.0 °C), and a full -3 °C scenario produced an indoor drop of 2.4 °C, reaching 26.4 °C. On the other hand, the +1 °C scenario raised the minimum temperature to 29.5 °C. The corresponding peak values are summarised in Figure 15. *EPW file modification for 1 °C decrease (CREDITS: CYPE)*, a reference for the comparative analysis between iterations.

Peak indoor minimum	Peak indoor minimum comfort temperature results for EPW file variations				
Iteration (Step)	Ambient temperature variation (°C)	Peak indoor minimum comfort temperature (°C)			
Base (3)	-	28.8			
1 st modification (4) _a	-1 °C	28.0			
2 nd modification (4) _b	-2 °C	27.2			
3 rd modification (4) _c	-3 °C	26.4			
4 th modification (4) _d	+1 °C	29.5			

Table 15. Peak indoor minimum comfort temperature results for EPW file variations

Table 15 shows that for both maximum and minimum temperatures, the trend showed a linear and predictable indoor response to changes in external temperatures, which implies that even marginal improvements to pavement thermal properties could propagate as consistent indoor comfort benefits. The parallelism also confirms the stability of the building envelope and internal zoning configuration used in the model, validating the selected workflow and tool capabilities for early-stage testing. This allows for more confident extrapolation of results to real-world UHI mitigation planning and design assessments.

6.2. DATA-DRIVEN DIGITAL TOOL



As part of the testing and validation of the data-driven digital tool prior to its implementation at the Spanish demo site, a series of tests were carried out.

The following sections describe the data used for these tests, present the results of applying the automated RC modelling engine to the test dataset, and compare them with manually calibrated models.

6.2.1. TESTING DATASET

The data used during task 4.3 of the project for the first tests of the tool corresponded to a dike in the Netherlands. In the second phase of the project a different dataset has been used to test the data-driven digital tool.

The grant agreement of the project described a experimental campaign to be carried out in Tecnalia's facilities, in the experimental infrastructure Kubik (Garay et al.), to obtain the dataset to be used for the test of the tool. Even though, due to external circumstances affecting the acquisition process of the required sensors, it was not possible to conduct a sufficiently long monitoring campaign. To overcome this limitation, data collected at COMSA's facilities from the monitoring of various pavement samples during Task 9.2 has been used instead.

Each of the monitored samples has the same standard pavement section of the streets of Barcelona (Figure 24). Three different asphalt mixes have been applied on them. Specifically, two formulations or mixes have been designed and mechanically tested for the wearing course, which will be compared with a mechanically equivalent standard mix. The wearing course for each of the three samples are as follows:

- Mix 1: baseline (asphalt concrete mix in Barcelona) for comparison.
- Mix 2: 25% recycled glass in the sand fraction with normal aggregates.
- Mix 3: 20% recycled glass in the sand fraction with white aggregates.



Figure 24. Layout of the three pavement samples monitored in Barcelona (CREDITS: COMSA)

All the samples present the same monitored variables (Figure 25). Four temperature sensors (a type T thermocouple was used, with a 4x30 mm stainless steel sheath, 2 m of Teflon/silicone cable, and a type T Mini b compensated connector compatible with the Multilogger M1200E of COMET) were installed in each of the samples, with a distribution that guarantees the correct measuring of the whole surface. The sensors were placed at the interface between the cold pavement wearing course and the underlying AC22 layer, ensuring an accurate monitoring of temperature variations at this critical junction.



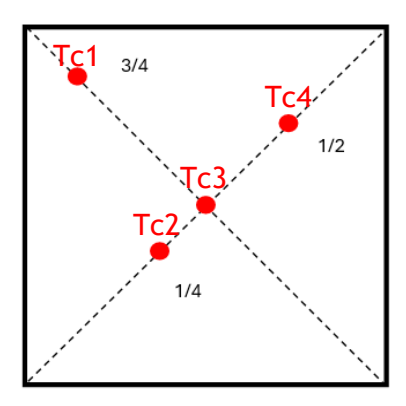


Figure 25. Temperature sensor distribution (CREDITS: COMSA)

Since for the evaluation of the digital tool it is not important to improve the thermal properties of the modelled sample, for the sake of simplicity the tests have been carried out with data corresponding to the baseline sample (mix 1). Weather data used in this evaluation process has been obtained using the Weatherbit API (*Historical Weather API* | *Weatherbit*) and the location of the experiment (41.575, 1.922).

The monitored data cover a period spanning from 2024-07-14 to 2024-11-18, with an hourly frequency. Figure 26 illustrates the monitored slab temperature data, along with the corresponding solar radiation and ambient temperature values, for a typical summer week extracted from this period. As shown in Table 16, the measurements from all 4 sensors exhibit minimal variability. Therefore, from here onward the mean value of all sensors will be used as the representative actual monitored surface temperature value.

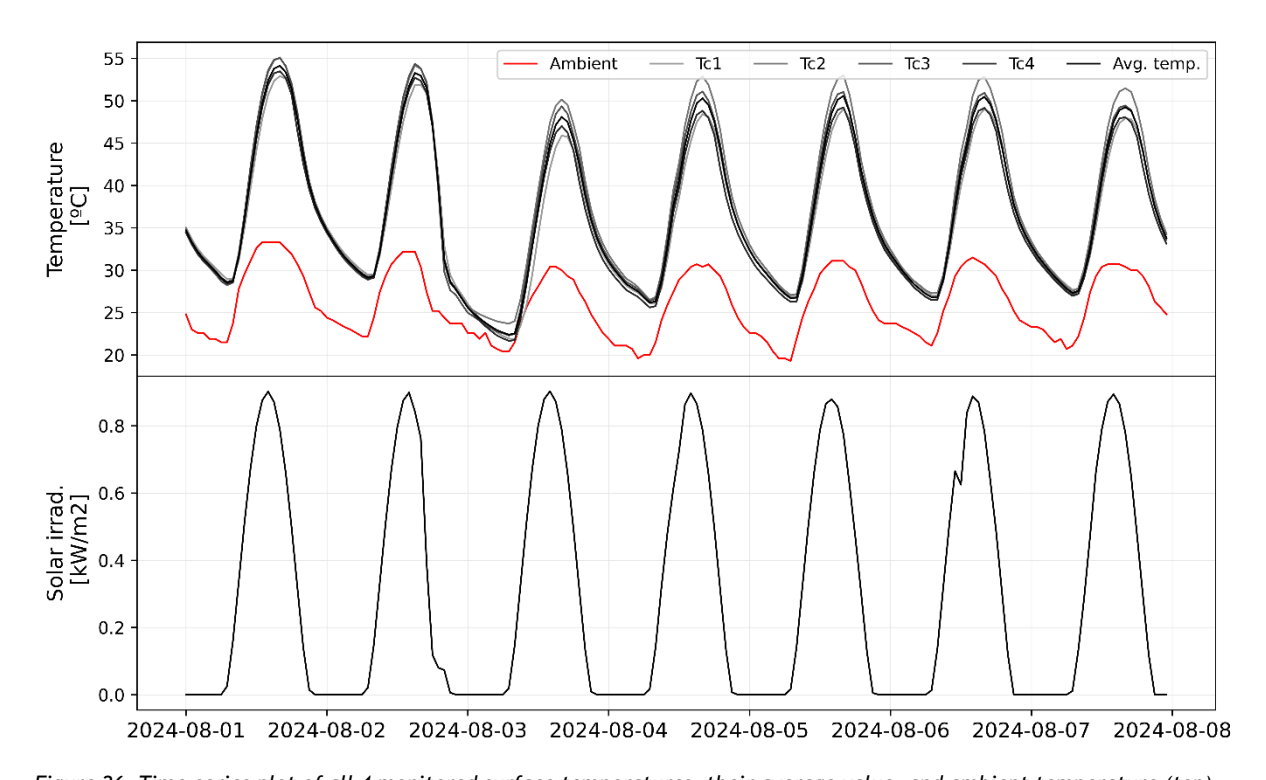


Figure 26. Time-series plot of all 4 monitored surface temperatures, their average value, and ambient temperature (top), and solar irradiation (bottom) (CREDITS: TECNALIA)



	TCI [°C]	TC2 [°C]	TC3 [°C]	TC4 [°C]
Quantile = 25	17.95	18.18	17.83	17.75
Quantile = 50	25.38	26.05	25.51	25.40
Quantile = 75	32.57	33.70	32.98	32.34
Max	53.52	55.95	55.58	54.35
Min	8.82	8.55	8.47	8.53

Table 16. Statistical comparison of measured temperature values

6.2.2. RESULTS OF DATA-DRIVEN DIGITAL TOOL

In this section, the results of the application of the RC model generator tool are shown. As in the preliminary tests performed during Task 4.3, the tool starts fitting the simplest model (1 node) and keeps on adding more complexity until nonsignificant improvements are found in the bigger model.

Figure 27 shows as an example a subset of the structure of various possible models. Like in the application case described in D4.3, all topologies are restricted to maintain a certain degree of interpretability, resulting in a single possible model for each number of nodes.

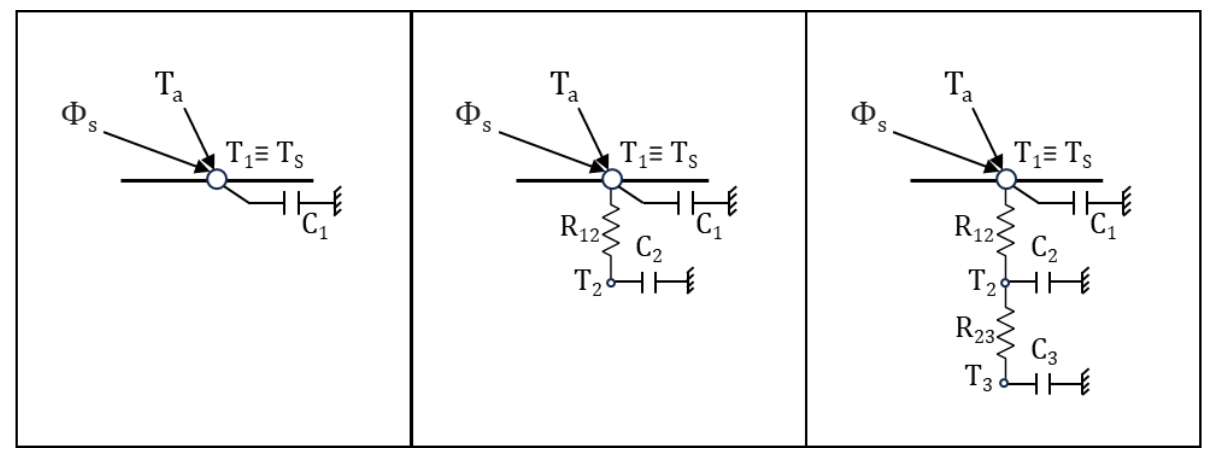


Figure 27. Subset of possible topologies of the optimal model: 1 node RC model (left), 2 nodes RC model (middle), 3 nodes RC model (right) (CREDITS: TECNALIA)

In addition to the information criteria described in Section 4.1.2 as the main indicator used to compare different models, several commonly used metrics (Song et al.) are also calculated to facilitate the analysis of the accuracy of the built models.

Three different error metrics are used: the mean absolute error (MAE, Eq. (7)), the root mean square error (RMSE, Eq. (8)), and the coefficient of determination $(R^2, Eq. (9))$. The first two metrics quantify the discrepancies between predicted and actual values. While the MAE assigns equal weight to all errors, the RMSE gives more weight to larger errors, making it more sensitive to outliers. On the other hand, R^2 is used to assess the model goodness of fit. Its value represents the proportion of variance in the observed data that is explained by the model, with higher values indicating a closer alignment between predicted and actual values.



$$MAE = \frac{1}{n} \sum_{i=1}^{n} |y_i - \widehat{y}_i| \tag{7}$$

$$RMSE = \sqrt{\frac{1}{n} \sum_{i=1}^{n} |y_i - \widehat{y}_i|^2}$$
 (8)

$$R^{2} = 1 - \frac{\sum_{i=1}^{n} (y_{i} - \hat{y}_{i})^{2}}{\sum_{i=1}^{n} (y_{i} - \overline{y})^{2}}$$
(9)

The automated RC model generator engine is applied to the dataset described in Section 6.2.1 *Testing dataset*. The algorithm outlined in Figure 28. *Algorithm for automated pavement model selection (CREDITS: TECNALIA)* is iteratively executed until the optimal model is identified. Figure 17. *Hourly surface temperature variation by conductivity and hybrid iterations (CREDITS: CYPE)* presents a summary of the error metrics calculated for each of the identified models. Among these, the 3-node model is selected as the best compromise between accuracy and complexity, the model that presents a lower BIC value.

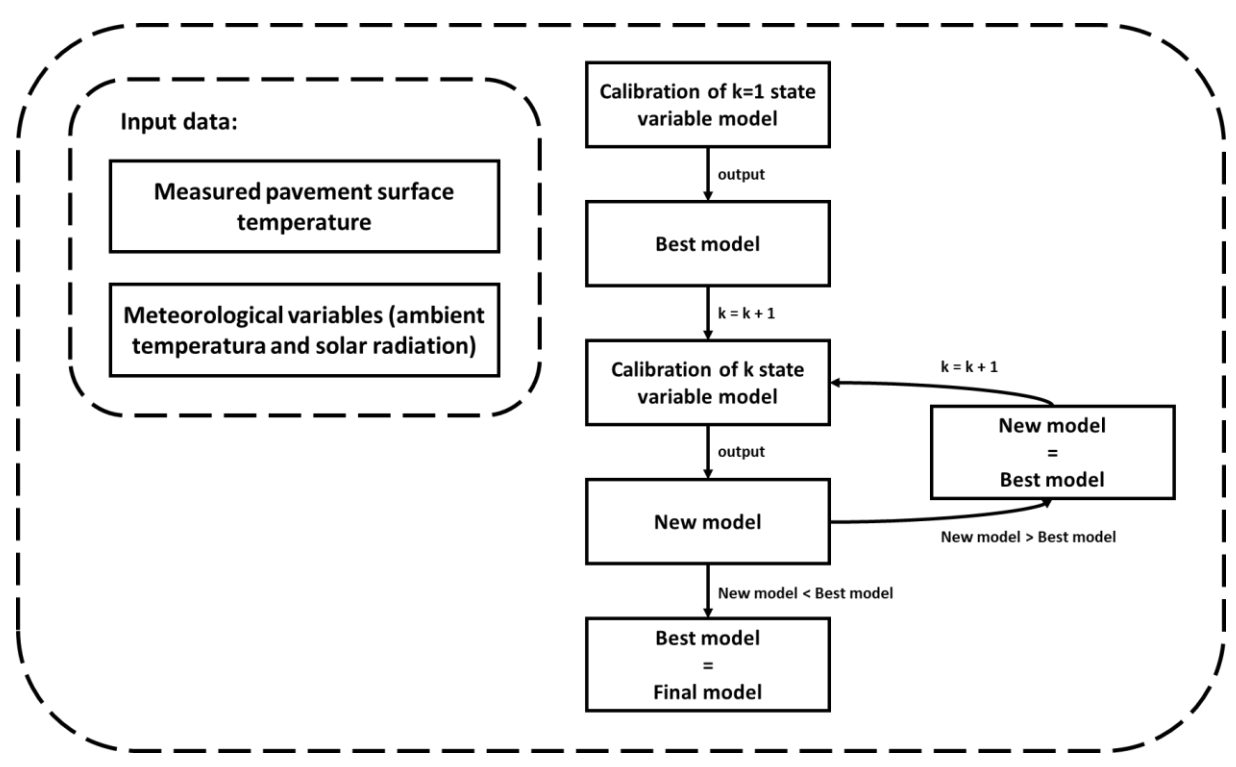


Figure 28. Algorithm for automated pavement model selection (CREDITS: TECNALIA)

N° of nodes of the model	N° of parameters	R ²	MAE [°C]	RMSE [°C]	BIC
1 node	3	0.9817	1.0290	1.4663	8927.3010
2 nodes	5	0.9950	0.4798	0.7706	4272.7180
3 nodes	7	0.9952	0.4654	0.7488	4075.9402



4 nodes 9 0.9952 0.4654 0.7488 410	.2361	
------------------------------------	-------	--

Table 17. Evaluation metrics of all identified RC models

Figure 29 displays the predicted and residual values for a typical summer week in Barcelona. The residual plot reveals that the model accurately captures peak temperature values. The variability in residuals exhibits a strong correlation with fluctuations in solar irradiation, without significantly affecting the model ability to predict the highest monitored temperature values, which are the most critical from a heat island effect perspective.

On the other hand, Figure 30 illustrates the model performance during a cloudy summer period. Similar to the previous figure, the model accurately predicts peak temperature values. However, its accuracy is somewhat reduced when faced with fluctuations in solar irradiation variable, i.e., in cloudy periods. Despite this, the largest residuals remain within acceptable limits for the application of the model, and it is worth noting that these periods of lower accuracy typically coincide with conditions where the heat island effect is less pronounced.

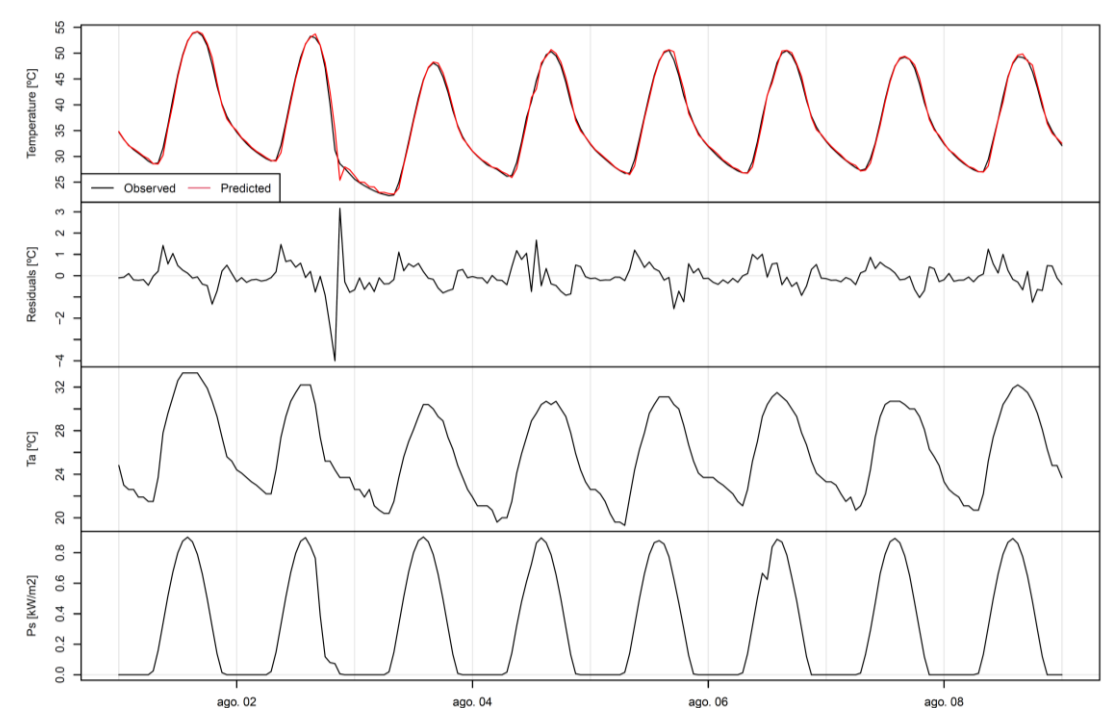


Figure 29. Time-series plots of observed versus predicted temperature values, residuals, ambient temperature (Ta), and solar irradiation (Ps) for a typical summer week (CREDITS: TECNALIA)



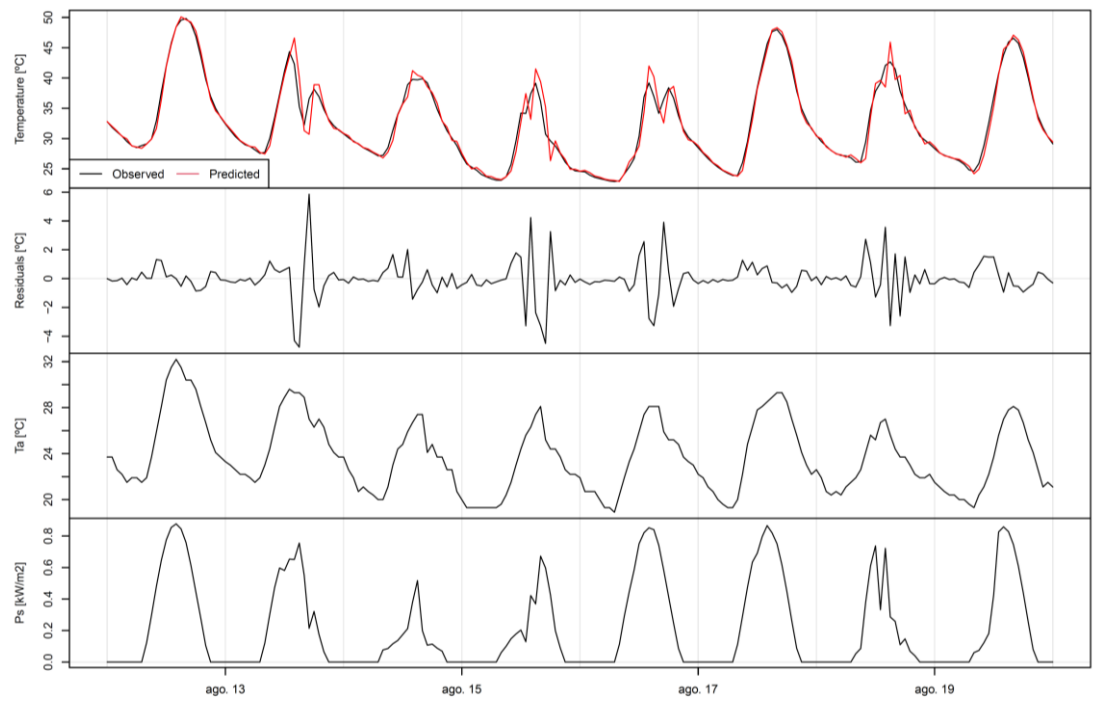


Figure 30. Time-series plots of observed versus predicted temperature values, residuals, ambient temperature (Ta), and solar irradiation (Ps) for a cloudy period (CREDITS: TECNALIA)

6.2.3. COMPARISON VS MANUALLY CALIBRATED RC MODEL

The algorithm described in Figure 28 is applied manually using the CTSMR software until the optimal model is identified. Given the differences in the calibration process and the use of the CTSMR software, it can be assumed that there is not a unique solution for each model even if both approaches share the same dataset. Table 18 includes the error metrics calculated for all 4 models and shows the differences between these models and the ones identified by the automated model generator engine. In contrast with what was seen in the previous section, in the case of the manually calibrated models, the one that shows the best metrics, both from an accuracy and complexity perspective, is the 2-node model.

N° of nodes of the model	N° of parameters	R²	MAE [°C]	RMSE [°C]	BIC
1 node	3	0.9816	1.0350	1.4686	11880.5237
2 node	5	0.9950	0.4816	0.7749	7477.8163
3 node	7	0.9916	0.6919	0.9944	9380.1792
4 node	9	0.9917	0.6877	0.9877	9183.8072

Table 18. Evaluation metrics of all manually identified RC models

A detailed analysis, depicted in Figure 31 and Figure 32, of the accuracy of the manually calibrated 2 nodes model in the same two periods analysed in Section 0 leads to the same conclusions as those of the automatically obtained 3 nodes model. In fact, when comparing the plots of both models it can be seen that they show almost the exact outputs, both qualitatively and quantitatively. This proves that the models built by the automated RC generator engine are, at least, as good as the ones identified manually.



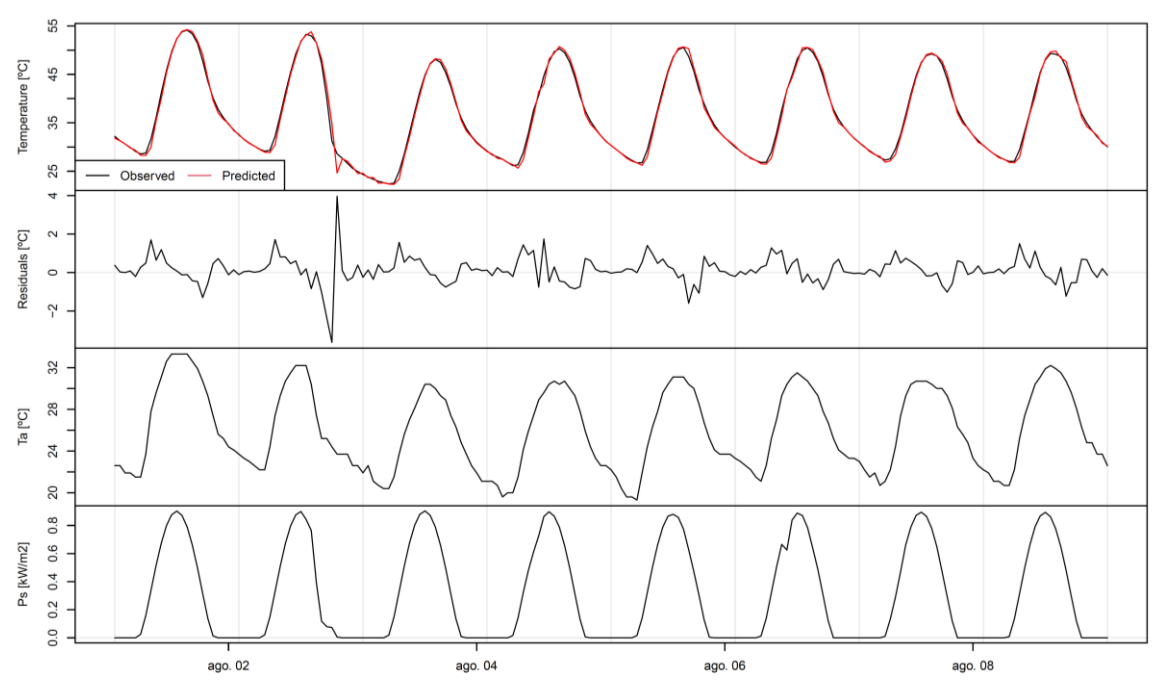


Figure 31. Time-series plots of observed versus predicted (manually calibrated) temperature values, residuals, ambient temperature (Ta), and solar irradiation (Ps) for a typical summer week (CREDITS: TECNALIA)

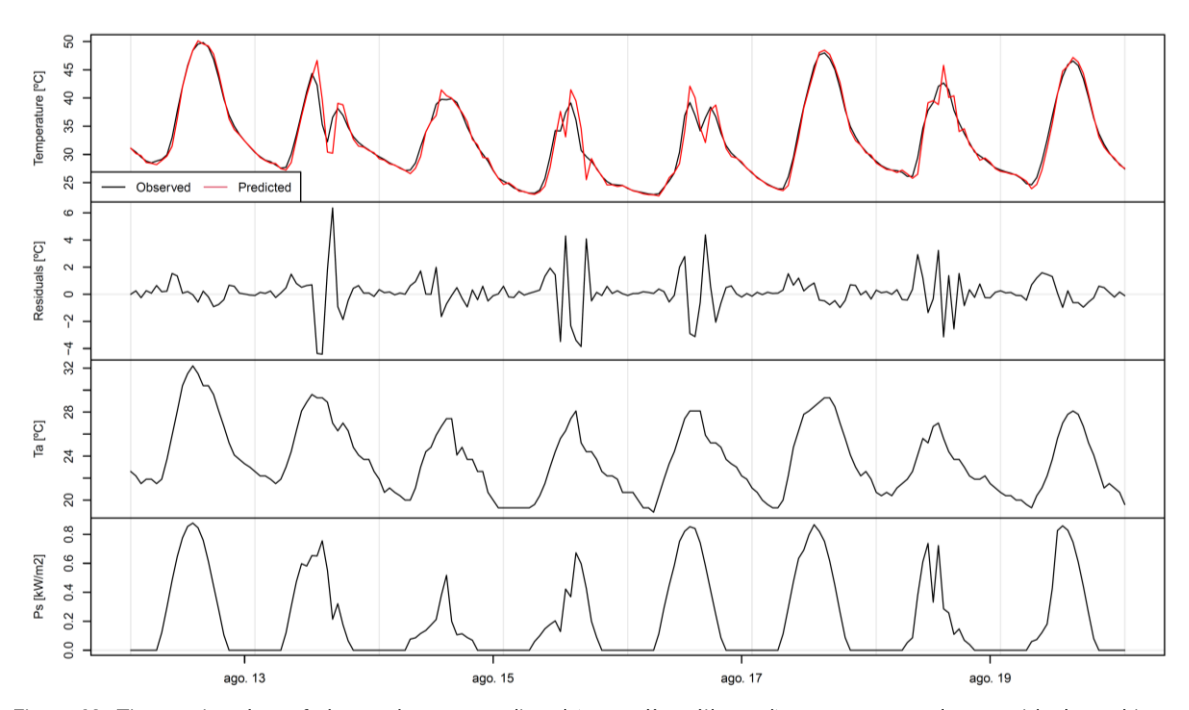


Figure 32. Time-series plots of observed versus predicted (manually calibrated) temperature values, residuals, ambient temperature (Ta), and solar irradiation (Ps) for a cloudy period (CREDITS: TECNALIA)



7. DEVIATIONS TO THE PLAN

The development of the task has experienced two main deviations from what was specified in the Grant Agreement, each affecting one of the digital tools.

The first deviation concerns the final location of the Spanish demo site. As stated throughout this document, there is currently no officially confirmed location, with several possible options still under consideration. This uncertainty has impacted the initial testing of the physics-based digital tool, which was intended to model the Spanish demo site. To address this issue, the physics-based tool was tested using a hypothetical site location, allowing its functionality to be validated despite the lack of a final site.

The second deviation involves a delay in the start of the monitoring campaign planned at Tecnalia's Kubik test building facilities. Due to external circumstances affecting the acquisition process of the required sensors, it was not possible to conduct a sufficiently long monitoring campaign. The data from this campaign was intended to validate the final design of the data-driven digital tool. To overcome this limitation, data acquired at COMSA's facilities, during the monitoring of various pavement samples, was used instead. Furthermore, due to the final design of the tool and contrary to what was specified in the grant agreement, it has not been necessary to have data related to energy consumption available.



8. CONCLUSIONS

The two digital tools developed and presented in this deliverable, physics-based and data-driven, demonstrate significant advances in urban climate adaptation analysis, specifically focused on the thermal characterisation of pavement materials and their impact on building energy performance. Although each tool follows a different methodology and serves a different purpose, they are both aligned with MULTICLIMACT's broader goal of providing stakeholders with replicable tools to evaluate and design resilient urban interventions.

The simultaneous development and testing of both tools within Task 10.3 confirm their readiness for future real-case applications. The **physics-based tool** enables a **consistent scenario modelling at urban scale** with minimal reliance on external resources. On the other hand, the **data-driven** tool introduces an **accessible**, **low-threshold approach** to develop data-based models and KPIs, using an RC model generator as its main engine. The two developed digital tools address different phases in the evaluation of the designed and installed solutions, providing valuable insights both at the **design stage** (physics-based tool) and during **actual use** (data-driven tool).

Throughout the physics-based modelling development process, continuous testing and simulation were conducted to prove the tool improved functionalities and validate the performance and accuracy of the workflow, prior further real-case simulations on future tasks.

The thermal properties of different pavement configurations were tested and analysed for their integration into the model. This allowed for a more accurate representation and simulation of potential ground-level heat behaviour within the urban context. Energy simulations were also performed to verify the proper functioning of the workflow. These early-stage tests were key in confirming the tool ability to simulate both existing conditions and the effects of proposed solutions, prior the final selection of the demo site and the full-scale application of the modelling strategy in a real-world scenario. Early simulations using these theoretical scenarios suggest that the model behaves as expected and produces coherent results. The process has proven to be robust, replicable and manageable, eliminating the need for external software interventions.

Moreover, by simulating various possible scenarios and varying the pavement material property values, a general understanding and indicative **thresholds** of how the actual proposed solution may behave can be obtained. This might serve as a reference parameter or target range for the expected results that the final monitored data from the demo site should fall within, once available. These preliminary insights are valuable for **guiding expectations**, **informing calibration procedures**, **and supporting the comparative analysis** between simulated and observed behaviour during the next project phases.

Regarding the simulation results, it can be concluded that the **most influential parameter** in pavement thermal behaviour is the **surface absorptance**. Simulations demonstrated than even small reductions in absorptance (i.e., increasing reflectivity or albedo) meant considerable drops in surface temperature and heat flux, helping **mitigate heat accumulation and energy release** to the surrounding air. On the other hand, while not as significant as absorptance, thermal conductivity also influenced the overall results, by affecting the rate and depth of heat transfer within the pavement body, moderating surface peaks, and influencing dissipation profiles, especially in the evening.

Additionally, the influence of pavement temperature on indoor conditions and building energy demand was confirmed through simulations using modified EPW files. Cooling demand showed a steady and predictable reduction when pavement-induced ambient temperatures were lowered. While heating needs increased proportionally, this trade-off is consistent with the thermal dynamics of Mediterranean climates. Importantly, operative temperatures inside buildings responded linearly to changes in external conditions, validating the workflow and reinforcing the role of pavement design as a strategy to improve thermal comfort.

On the other hand, the work related to the data-driven digital tool in this task focused on further



developing the preliminary design presented in Deliverable D4.3 during the first year of the project. A detailed analysis of the potential KPIs that the tool could produce was carried out, leading to the selection of **operative temperature** as the most suitable output. To enable the calculation of operative temperature, a literature review was conducted to identify the most appropriate method for estimating **sky temperature**, which is a critical input for the selected KPI.

During Task 10.3, a new dataset was used to validate the data-driven tool. Unlike the first phase of the project, where soil data was employed, this phase utilized monitored data from a **pavement sample**. This new dataset enabled the finalization of the tool design.

The validation results show that hybrid models are highly effective in characterizing the thermal behaviour of pavement solutions. Moreover, the **automated RC model generation engine** greatly simplifies what would otherwise be a complex model identification process. Although **this aspect lies beyond the scope** of the present project, it holds potential for the development of advanced predictive models. Such models could be leveraged by smart control systems to **operate active technologies**, including HVAC systems and shading devices.

For both tools, final validations will be completed in **Tasks 11.2 and 15.2** using real data from the pavement solutions and the selected demo case geometry.

Finally, the tools developed under Task 10.3 of MULTICLIMACT are now **technically mature** and **aligned with the project goal of supporting urban climate adaptation** with evidence-based, user-friendly digital solutions. Their distinct but at the same time complementary approaches offer a strong foundation for future demonstration activities, where their capabilities will be tested in **real scenarios** and further refined. By combining simulation-based foresight with data-based validation, these tools contribute decisively to bridging the gap between design intentions and actual urban performance.



9. LITERATURE /REFERENCES

Bliss, Raymond W. "Atmospheric Radiation near the Surface of the Ground: A Summary for Engineers". *Solar Energy*, vol. 5, no. 3, 1961, pp. 103-20. *ScienceDirect*, https://doi.org/10.1016/0038-092X(61)90053-6.

Brutsaert, Wilfried. "On a Derivable Formula for Long-Wave Radiation from Clear Skies". *Water Resources Research*, vol. 11, no. 5, 1975, pp. 742-44. *Wiley Online Library*, https://doi.org/10.1029/WR011i005p00742.

"CYPETHERM EPlus". *CYPE*, https://info.cype.com/en/product/cypetherm-eplus/. Accessed 21 Jul. 2025.

Dilley, AC, and D. O'brien. "Estimating Downward Clear Sky Long-wave Irradiance at the Surface from Screen Temperature and Precipitable Water". *Quarterly Journal of the Royal Meteorological Society*, vol. 124, 2006, pp. 1391-401. *ResearchGate*, https://doi.org/10.1002/qj.49712454903.

Evangelisti, Luca, et al. "On the Sky Temperature Models and Their Influence on Buildings Energy Performance: A Critical Review". *Energy and Buildings*, vol. 183, 2019, pp. 607-25. *ScienceDirect*, https://doi.org/10.1016/j.enbuild.2018.11.037.

Garay, Roberto, et al. "Energy Efficiency Achievements in 5 Years Through Experimental Research in KUBIK". *Energy Procedia*, 6th International Building Physics Conference, IBPC 2015, vol. 78, 2015, pp. 865-70. *ScienceDirect*, https://doi.org/10.1016/j.egypro.2015.11.009.

Historical Weather API | *Weatherbit*. https://www.weatherbit.io/api/historical-weather-api. Accessed 8 Jul. 2025.

"ISO 13790:2008". ISO, https://www.iso.org/standard/41974.html. Accessed 21 Jul. 2025.

Lopez-Villamor, Iñigo, et al. "Time of the Week AutoRegressive eXogenous (TOW-ARX) Model to Predict Thermal Consumption in a Large Commercial Mall". *Energy Conversion and Management: X*, vol. 24, Oct. 2024, p. 100777. *ScienceDirect*, https://doi.org/10.1016/j.ecmx.2024.100777.

Prata, A. J. "A New Long-Wave Formula for Estimating Downward Clear-Sky Radiation at the Surface". *Quarterly Journal of the Royal Meteorological Society*, vol. 122, no. 533, 1996, pp. 1127-51. *Wiley Online Library*, https://doi.org/10.1002/qj.49712253306.

Schwarz, Gideon. 'Estimating the Dimension of a Model'. *The Annals of Statistics*, vol. 6, no. 2, Mar. 1978, pp. 461-64. *Project Euclid*, https://doi.org/10.1214/aos/1176344136.

Song, Jiancai, et al. 'Predicting Hourly Heating Load in a District Heating System Based on a Hybrid CNN-LSTM Model'. *Energy and Buildings*, vol. 243, Jul. 2021, p. 110998. *ScienceDirect*, https://doi.org/10.1016/j.enbuild.2021.110998.

Staley, D. O., and G. M. Jurica. *Effective Atmospheric Emissivity under Clear Skies*. Mar. 1972. Journal of Applied Meteorology and Climatology. *journals.ametsoc.org*, https://journals.ametsoc.org/view/journals/apme/11/2/1520-0450_1972_011_0349_eaeucs_2_0_co_2.xml.

Tabrizi, Sepideh Emami, et al. 'Hourly Road Pavement Surface Temperature Forecasting Using Deep Learning Models'. *Journal of Hydrology*, vol. 603, Dec. 2021, p. 126877. *ScienceDirect*, https://doi.org/10.1016/j.jhydrol.2021.126877.

Vetter, Phillip, et al. ctsmTMB: Continuous Time Stochastic Modelling Using Template Model Builder. Version 1.0.0, 8 Apr. 2025. R-Packages, https://cran.r-project.org/web/packages/ctsmTMB/index.html.

Zhang, Kun, et al. Sky Temperature Estimation and Measurement for Longwave Radiation Calculation. 2017. ResearchGate, https://doi.org/10.26868/25222708.2017.569.



